Applied Geochemistry 160 (2024) 105836

Contents lists available at ScienceDirect

Applied Geochemistry

journal homepage: www.elsevier.com/locate/apgeochem

Vertical and lateral distribution of helium in porewater of the Mesozoic sedimentary sequence of northern Switzerland – A comparative investigation across multiple boreholes

D. Rufer [a,*], H.N. Waber [a,b], D. Traber [c]

[a] Rock-Water Interaction (RWI), Institute of Geological Sciences, University of Bern, CH-3012, Bern, Switzerland
[b] WaterGeoChem Consulting, CH-3013, Bern, Switzerland
[c] Nagra, CH-5430, Wettingen, Switzerland

ARTICLE INFO

Editorial handling by Dr. E. A. C. Neeft

Keywords:
Helium
Dissolved noble gas
Porewater chemistry
Groundwater
Diffusion
Cross-formation gas transport
Swiss deep drilling programme

ABSTRACT

Helium concentrations and $^3He/^4He$ ratios were measured on porewater extracted from the low-permeability rock matrix and groundwater in bounding aquifers in Northern Switzerland. The samples were collected from six deep boreholes, which were drilled across the Tertiary Molasse and the underlying Mesozoic sediments at three different study areas within the context of Nagra's deep drilling programme for the underground disposal of radioactive waste. Porewater helium data obtained from each borehole at high spatial resolution describe continuous profiles over multiple aquifer-aquitard intervals across the Jurassic to Triassic sediment sequence. Given the lateral distribution of the investigated areas (~20 km apart) and having two boreholes in each area (a few km apart), this allows to investigate both vertical and lateral changes of He in the porewater and groundwater system at high resolution and over large scales.

In the about 300–400 m thick Dogger–Lias aquitard sequence including the Opalinus Clay, porewater He concentrations are nearly identical and have very similar $^3He/^4He$ signatures in all boreholes. This suggests a common history in the development of these systems despite the boreholes being located in three study areas with different hydrogeological setting and tectonic history since their last burial and diagenesis. Proximal to the groundwaters, He profiles show that the porewater system is controlled by diffusive redistribution of in-situ produced He from high concentrations in the aquitards towards lower concentrations in the bounding groundwaters. At some locations, the influence of evaporitic strata with very low diffusivity acting as transport barriers becomes obvious. Close to the aquitards, differences between the profile shapes of helium and other conservative tracers such as δ^2H in the different boreholes and areas indicate different boundary conditions for the different tracers over the more recent geological past, as well as, for some boreholes, the potential contribution of helium from the groundwater to the porewater in the nearby low-permeability rock matrix.

In one study area, cross-formation transport of helium could be identified close to a deep reaching tectonic structure related to the Hegau-Lake Constance fault system. This basement derived gas is subsequently laterally distributed via groundwater in the different aquifers and influences the porewater of the adjacent aquitard formations, as evidenced by the helium concentrations and $^3He/^4He$ ratios in the groundwater and porewater in the two boreholes of this siting area.

1. Introduction

Clay-rich rocks are important barriers for fluid flow and act as aquitards separating water conducting formations. Their very low hydraulic conductivity, coupled with good chemical retention properties for cationic contaminants makes them ideal seals for waste deposits. For these reasons, they are being investigated by many countries as potential host rocks for the underground disposal of radioactive waste (e.g., Gautschi, 2017; Ondraf/Niras, 2001; Nagra, 2002; Andra, 2005; Delay et al., 2008; Hendry et al., 2015). In this context, helium is a powerful tracer to investigate hydrogeological processes and solute transport in such aquitard – aquifer systems due to its chemical inertness, low

* Corresponding author. Institute of Geological Sciences, Baltzerstrasse 1+3, CH-3012, Bern, Switzerland.
E-mail address: daniel.rufer@unibe.ch (D. Rufer).

https://doi.org/10.1016/j.apgeochem.2023.105836
Received 25 February 2023; Received in revised form 1 September 2023; Accepted 8 November 2023
Available online 22 November 2023

abundance in air and air-saturated water and high diffusivity in porewater. Furthermore, He is produced by in-situ geogenic production, therefore complimenting other tracers with similar transport properties such as stable isotopes of the water molecule in temporally constraining hydrogeological processes. Examples of where helium has been used to investigate various hydrogeological settings in the past comprise the Triassic sedimentary sequence in Morsleben, Germany (Osenbrück et al., 1998), the Jurassic Callovo-Oxfordian shale (Bigler et al., 2005) and deeper lying Triassic sediments (Battani et al., 2011; Jean-Baptiste et al., 2016; Waber, 2012) in the Paris Basin, the fractured Jurassic Tournemire shale in Southern France (Bensenouci et al., 2011), the Oligocene Boom Clay in Belgium (Mazurek et al., 2009), the Jurassic Opalinus Clay in the Swiss Molasse Basin (Nagra, 2001; Rufer and Waber, 2015) and in the folded Jura Mountains at Mont Terri (Rufer et al., 2018; Rübel et al., 2002; Waber and Rufer, 2017), the Permian sediment sequence in the Swiss Molasse Basin (Tolstikhin et al., 1996, 2011) as well as the Ordovician shale in the Michigan Basin, Canada (Clark et al., 2013). For the Callovo-Oxfordian shale, the Boom Clay and the Opalinus Clay, Mazurek et al. (2009, 2011) provide a comprehensive data compilation of helium and other tracer data, including transport modelling approaches, from studies existing until 2009.

Between 2019 and 2022, Nagra (the Swiss National Cooperative for the Disposal of Radioactive Waste) conducted a deep drilling campaign in the context of their site selection programme for a deep geological repository for radioactive waste in northern Switzerland (TBO programme, see Mazurek et al., 2023, Fig. 1). As a part of the hydrogeochemical investigations into the porewater and groundwater situation, properties and evolution within the Triassic-Jurassic aquitard sequence and its bounding aquifers, six out of nine boreholes were extensively sampled for dissolved noble gases in the rock's porewater. Here we present and discuss helium concentration and helium isotope composition profiles in porewater and groundwater obtained at high resolution from these boreholes. These profiles a) contribute to locate water conducting zones that limit the thickness of the aquitard but cannot be directly pinpointed due their low hydraulic conductivity preventing groundwater sampling, b) allow to characterise lateral differences with respect to the hydrogeological system and solute transport properties between boreholes as well as between study areas and c) allow to interpret their shape with respect to hydrogeological interactions between the porewater of the aquitard and changing boundary conditions in the aquifers over time. In addition, parent radionuclide concentrations measured in the various sedimentary strata encountered

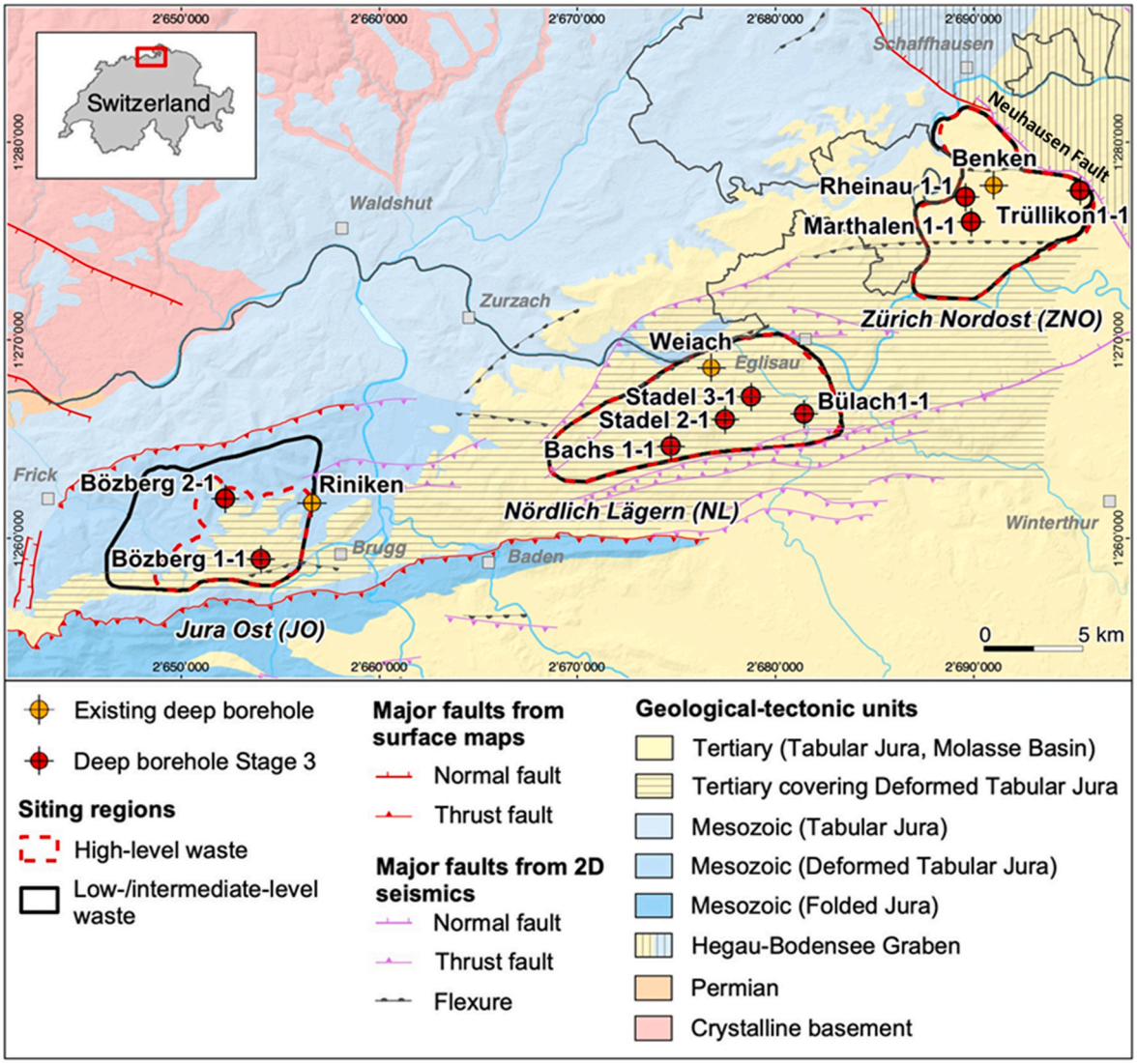

Fig. 1. Geological-tectonic map with locations of study areas, boreholes and tectonic features mentioned in this study (adapted from Madritsch 2015)
The existing boreholes Schlattingen and Oftringen are located approximately 6 Km NE of borehole Trüllikon 1-1 and 25 km SW of borehole Bözberg 1-1; the TBO boreholes Bachs 1-1, Stadel 2-2 and Rheinau 1-1 were not sampled for noble gases.

in the boreholes enable calculating the in-situ geogenic production of ^{4}He and its accumulation in the porewater, allowing to calculate timescales for the diffusive transport of helium in these sediments. This highly resolved dataset, which, together with the geographic distribution of the boreholes and the availability of a large set of other chemical and isotopic tracers in porewaters and groundwaters as well as their diffusive transport parameters (Mazurek et al., 2023 and references therein), holds the potential for an integrative interpretation of the porewater and groundwater system and its evolution in this part of northern Switzerland, as well as providing valuable information about long-term solute transport across these potential host rock strata. While some literature data concerning noble gases in porewaters is available for northern Switzerland (boreholes Benken (Nagra, 2001); Oftringen (Waber, 2008); Schlattingen (Rufer and Waber, 2015) and Weiach (Tolstikhin et al., 2011, 2018)), the datasets are limited and the boreholes are – with exception of the Benken and Weiach boreholes – located outside the study areas investigated here (Fig. 1). While this existing data is cardinally comparable with the presented TBO data, it is only used or referred to in specific, appropriate cases in this study. The same applies to similar data from Mont Terri or other sedimentary units investigated for noble gases.

2. Geological and hydrogeological setting

Three study areas along the northern edge of the Swiss Molasse Basin were investigated - from west to east; Jura Ost (JO), Nördlich Lägern (NL) and Zürich Nordost (ZNO) (Fig. 1). These study areas are situated in different tectonic regimes with JO being situated in the Deformed Tabular Jura Mountains whereas in NL and ZNO the sediment pile is unfolded and flat lying. In all three areas, the investigated strata start in the Jurassic sediments of the carbonaceous and marly units in the Malm and continue down into the aquitard sequence of the Dogger and Lias (Fig. 2). The Dogger is subdivided into a lithologically more heterogeneous upper part termed "Dogger above the Opalinus Clay" (D.A.O.) and the very homogeneous, clay-rich lower part formed by the Opalinus Clay (the potential repository host rock). A notable feature of the D.A.O. in NL is the presence of the Herrenwis unit, a reef-facies limestone with a thickness of approximately 40 m in the investigated boreholes of that area. The Opalinus Clay is underlain by the again lithologically more heterogeneous Liassic Staffelegg Formation. At the base, the boreholes were drilled at least into the heterogeneous Triassic groups of the Keuper and Muschelkalk. Keuper sediments consist of sandstone, dolomite and marls in the upper part (Klettgau Formation) and intercalated evaporite-marl layers in the lower part (Bänkerjoch Formation). The Muschelkalk consists mainly of dolomite and limestone at the top (Schinznach Formation), followed by evaporite layers (anhydrite and locally rock salt) in the Zeglingen Formation and argillaceous marls at the bottom (Kaiseraugst Formation). The Triassic sequence ends at the bottom with the sandstones of the Buntsandstein, which is underlain by Permian conglomerates (only in some boreholes) and the crystalline basement.

The Lias-Dogger aquitard sequence is bounded by an upper hydrogeological boundary in the Malm aquifer (ZNO and NL) or the Hauptrogenstein aquifer (located in the D.A.O., JO). The lower hydrogeological boundary is defined by either the local Keuper aquifer (which is not ubiquitously encountered in all boreholes based on lateral facies changes in the Klettgau Formation) or the regional Muschelkalk aquifer (Schinznach Formation), which forms the lowest boundary for natural tracer profiles across the Mesozoic sediment pile in all investigated boreholes. While this geologic setup forms a rough framework pertinent to all investigated boreholes, there are emphasised differences in the lithology and lithostratigraphy between the study areas as well as between individual boreholes. For a detailed geological setting, lithostratigraphy and details concerning the drilled boreholes, the reader is referred to Mazurek et al. (2023) and references therein; for details on the regional hydrogeology, see Gmünder et al. (2014), Nagra (2014), Waber and Traber (2022) and references therein.

3. Samples and methods

3.1. Sampling

Six boreholes (JO: BOZ1-1, BOZ2-1; NL: BUL1-1, STA3-1; ZNO: TRU1-1, MAR1-1) were investigated and 278 drillcore samples for the analysis of dissolved noble gases in porewater were taken at various depths. Sampling was performed using a spatially very dense sampling program that was designed to adaptively improve sampling resolution in stratigraphic sequences where changes in the noble gas inventory were expected e.g. due to observed or forecasted groundwater flow, in order to obtain a continuous and highly resolved geochemical dataset over the investigated sections of the boreholes.

Following a stringent protocol for sampling and recording sampling metadata as described in Rufer and Stockhecke (2021) served to preserve the in-situ water saturated state of the rock material, inhibit degassing of the dissolved gas and minimise potential sample contamination by extrinsic fluids or gases such as drilling mud or air. Strict adherence to these sampling protocols also facilitates forensic identification of potential causes for observed artefacts at a later stage. For noble gas samples, roughly 150 cm^3 cuboids were dry cut on site from the centre parts of lithologically homogeneous drillcore pieces shortly after extracting the cores from the core barrel to remove the potentially partly degassed and contaminated rim and top/bottom faces. After recording its wet weight, the cuboid was immediately sealed in a stainless-steel container with a ConFlat (CF) sealed lid fitted with an ultra-low leak rate, steel bellow-sealed valve and the entrapped air was removed by gently pumping the container to roughly 5–10% of the initial gas pressure followed by flushing with krypton (99.99% purity). This was repeated three times to efficiently pump off residual air without inducing significant sample degassing. Immediately afterwards the valve was closed and the sample container was stored at ambient temperature. Air exposure durations of the central cuboids before final sealing are narrowly confined, with an average of 8 min.

All depth measurements in this study are reported as meters below surface ("m MD"), which corresponds to measured depth along the drillpipe. With all investigated boreholes being vertical, this closely corresponds to true vertical depth.

3.2. Noble gas analysis of porewater

Determining porewater concentrations of dissolved noble gases is based on their quantitative release from the porewater (e.g. Osenbrück et al., 1998; Rübel et al., 2002) due to their low solubility in water under ambient conditions (Weiss, 1971). Their chemical inertness inhibits any reaction during out-gassing, allowing calculation of their porewater concentration from the released amount of gas and the mass of porewater of the rock sample.

Release of the dissolved gases from the porewater occurred by molecular diffusion into the container's void volume over the course of 4–26 months (median: 12 months) at a constant temperature of 20.5 ± 0.5 °C. Based on the diffusivity of helium and the size of the rock cuboids, it can be shown that less than 1% of helium stays dissolved in the porewater of sedimentary rocks (Bigler et al., 2005; Osenbrück et al., 1998). The released gas was extracted from the sample container by expansion and the sample container was then rapidly closed off to minimise artefacts due to pressure-change induced disturbances of the equilibrated gas composition. The sample gas was stripped of reactive gas phases using chemical getters operated at 280 °C (SAES st707) and ambient temperature (SAES GP50) and helium was separated from the heavy noble gases (including the Kr flushing gas) by a liquid-N_2 cooled cold trap filled with activated charcoal.

Amounts of ^{4}He were determined at the Institute of Geological Sciences, University of Bern, Switzerland, using a Hiden Analytical HAL 3F RC quadrupole mass spectrometer equipped with an in-line Faraday cup and CSEM detector, operated in static mode (Poole et al., 1997). About

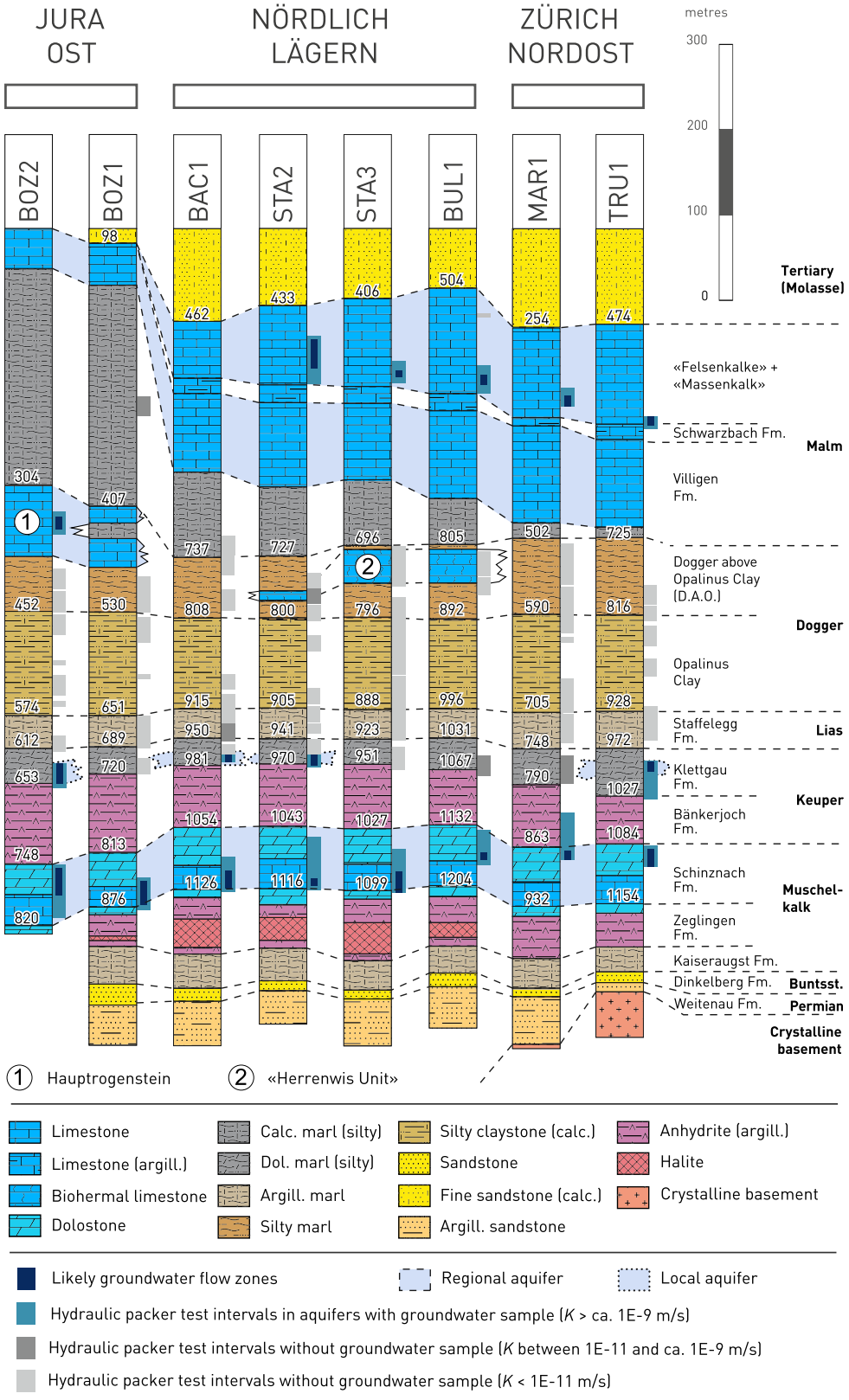

Fig. 2. Simplified lithostratigraphic profiles of all vertical boreholes drilled in the frame of the deep drilling project in 2019–2022, arranged from W (left) to E (right), from Mazurek et al. (2023).
Numbers indicate depths of selected stratigraphic boundaries in m below surface. Note that no hydraulic testing was performed in the Buntsandstein/crystalline basement and in the Tertiary Molasse sections, both of which may include horizons with enhanced permeability.

1/3rd of the samples were processed and analysed in duplicate, with obtained results overlapping within analytical uncertainty and average values being reported for these samples. The analyses were referenced against air (5.24 $\mu L_{He}/L_{air}$; de Laeter et al., 2003) and against two in-house standards of air enriched with 99.99 % pure He (isobaric, volumetric mixture) to 4360 $\mu L_{He}/L_{gas}$ and 1350 $\mu L_{He}/L_{gas}$ respectively, to roughly bracket the expected analyte concentration range in the sample gases. The latter standard was additionally strongly enriched in Kr to mimic the conditions of the Kr-flushed samples. For selected samples, a purified aliquot of He was analysed for $^3He/^4He$ ratios at the Institute of Environmental Physics, University of Bremen, Germany, according to the procedure given in Sültenfuss et al. (2009).

All concentrations of dissolved gases are reported in $cm^3(STP)_{gas}/g_{liquid}$ with the suffix for liquid being either porewater (pw) or groundwater (gw) and the standard temperature and pressure (STP) used for calculations being 273.15 K (0 °C) and 100 kPa (1 bar) according to the current definition by IUPAC (McNaught and Wilkinson, 1997). $^3He/^4He$ ratios are reported both as absolute values and relative to the atmospheric $^3He/^4He$ ratio (R/R_A), with $R_A = 1.34 \times 10^{-6}$ (current IUPAC reference value, Meija et al., 2016). No correction for contamination with air was performed for the helium data, as Ne concentrations measured on the same samples indicate that air-derived He (calculated using the atmospheric He/Ne ratio) accounts for less than 5‰ of the measured helium concentrations, which is roughly an order of magnitude lower than the propagated analytical uncertainty (for a discussion about air-contamination correction, see Rufer et al., 2018; Waber and Rufer, 2017). Analytical uncertainties are estimated using first order error propagation. Overall relative uncertainties on reported $^4He_{pw}$ values based on the combined propagated analytical uncertainties from noble gas analysis and the associated petrophysical measurements (see next section) are <35% for over 90% of the samples.

3.3. Petrophysical measurements

The mass of porewater, m_{pw}, was determined gravimetrically as the difference between the wet weight of the cuboid at the time of sampling on site, $m_{rock\ wet}$, and after gas-equilibration by drying in a ventilated oven at 105 °C until weight constancy was reached, $m_{rock\ dry\ (105°C)}$.

$$m_{pw} = m_{rock\ wet} - m_{rock\ dry\ (105°C)} \quad (1)$$

From this, the water content of the rock sample relative to its wet weight (W_{wet}), the sample wet density ($\rho_{bulk\ wet}$) and its water-loss porosity or volumetric moisture content (Φ_{WL}) are calculated as:

$$W_{wet} = \frac{m_{pw}}{m_{rock\ wet}} \quad (2)$$

$$\rho_{bulk\ wet} = \frac{m_{rock\ wet}}{V_{cuboid}} \quad (3)$$

$$\varphi_{WL} = \frac{W_{wet} * \rho_{bulk\ wet}}{\rho_{pw}} \quad (4)$$

where V_{cuboid} is the sample cuboid volume determined geometrically using its Cartesian dimensions and ρ_{pw} is the density of the porewater.

Based on porewater salinities determined on samples taken for hydrochemical analysis of the porewater (Wersin et al., 2023), the general porewater salinity in all six boreholes is sufficiently low to adopt a general porewater density of 1.0 g/cm^3 without introducing additional uncertainty. The notable exception to that is the BUL1-1 borehole, where drastically higher porewater salinities were measured in the upper Muschelkalk (Schinznach Formation). While high salinity (and the associated higher porewater density) affects the determination of various petrophysical properties such as W_{wet} and Φ_{WL} to some degree (for a discussion, see Mazurek et al., 2021), the conservatively estimated discrepancy between salinity-corrected and –uncorrected values does not exceed 15% for samples of the stratigraphic unit in this borehole. Considering this, as well as the issue that some of the porewater helium profiles extend beyond the depth range covered by the hydrochemical tracer profiles (and therefore no salinity data being available), no salinity correction was applied to the samples in this study and potential uncertainties linked to salinity were not taken into account. Analytical uncertaverainties are estimated using first order error propagation.

3.4. Analysis of radionuclide concentrations in bulk rock

Bulk rock concentrations of U and Th were measured by ActLabs, Ontario, Canada (www.actlabs.com) using sodium peroxide total fusion of the rock followed by ICP-MS analyses with lower detection limits of 0.1 ppm for U and Th, 15 ppm for Li and 0.1 wt% for K. A total of 64 representative bulk rock aliquots from drillcore samples covering the majority of lithologies encountered in the six boreholes were analysed. The sample material was selected from the central parts of the core sections to avoid potential contamination by drilling mud.

4. Results

4.1. Petrophysical data

For all investigated boreholes, the intensive properties ($\rho_{bulk\ wet}$, W_{wet} and Φ_{WL}) show fairly constrained ranges in more homogeneous, clay-rich sections such as the Opalinus Clay but a generally wider scatter in lithologically more heterogeneous sections. The latter pertains particularly to the rocks of the Bänkerjoch and Zeglingen formations due to the presence of anhydrite and locally occurring halite beds. The general quantitative ranges of these properties along a borehole profile are similar between boreholes within a specific study area and are tabulated as cumulative ranges per study area in Table 1. Overall, these values compare well with those obtained from neighbouring samples used for other porewater investigations (see Mazurek et al., 2023).

4.2. Bulk rock radionuclide content

The bulk rock samples analysed for radionuclide concentrations were specifically selected from boreholes BOZ1-1 and BOZ2-1 (JO, 23 samples), STA3-1 (NL, 19 samples) and MAR1-1 (ZNO, 22 samples) to cover all three study areas and the main lithologies encountered in the investigated boreholes. The summary data ranges for each stratigraphic unit per region are tabulated in Table 1.

4.3. Porewater helium data

Over all three study areas and all investigated boreholes (Figs. 1 and 2), the helium concentration profiles in the porewater show some clear similarities. Most strikingly are the near identical $^4He_{pw}$ concentrations in the Opalinus Clay and a predominantly flat profile shape in the central part of the aquitard formed by the low permeability, clay-rich Lias-Dogger sequence in all three study sites and in spite of the strongly different tectonic setting (Table 2). Comparing the shapes of the $^4He_{pw}$ profiles with those of the corresponding δ^2H profiles (Gimmi et al., 2023), a good correspondence over at least the Lias-Dogger aquitard section is observed. With increasing proximity to the groundwater occurrences above and below the aquitard, these profile shapes begin to diverge. There are further differences with respect to the $^4He_{pw}$ profile shape below the Keuper and when comparing porewater helium concentrations with those of the groundwaters, both within as well as between study areas.

4.3.1. Study area Jura Ost (JO)

The two boreholes BOZ1-1 and BOZ2-1 differ somewhat in terms of their helium porewater concentration profile (Fig. 3). BOZ1-1 features a uniform, straight profile from the top of the cored section in the Malm through the Dogger and Lias, with $^4He_{pw}$ values scattering narrowly around 2×10^{-3} $cm^3(STP)/g_{pw}$ (1.4×10^{-3} to 2.7×10^{-3} $cm^3(STP)/$

Table 1
Petrophysical and bulk rock radionuclide concentration summary data ranges and median values (in parentheses) of analysed samples per study area and stratigraphic unit.

		petrophysical properties						*bulk rock radionuclide concentrations*					
	Stratigraphy	**n**	**W_{wet}** [wt.%]		**$\rho_{bulk\ wet}$** [g cm^{-3}]		**$Ø_{WL}$** [vol.%]	**n**	**U** [mg kg^{-1}]		**Th** [mg kg^{-1}]	
Jura Ost (JO)	Malm	7	1.18 - 4.68	(3.90)	2.48 - 2.63	(2.53)	3.03 - 11.07 (9.38)	n.a.	n.a.		n.a.	
	D.A.O.	13	1.87 - 5.20	(3.93)	2.37 - 2.64	(2.52)	4.80 - 12.13 (9.50)	5	1.6 - 4.0	(3.0)	3.0 - 13.2	(5.3)
	Opalinus Clay	11	3.46 - 5.48	(4.73)	2.39 - 2.56	(2.49)	8.37 - 12.51 (11.27)	1	3.0		13.4	
	Staffelegg Fm.	5	3.68 - 5.88	(5.13)	2.29 - 2.51	(2.47)	8.74 - 13.43 (11.79)	1	3.1		10.9	
	Klettgau Fm.	5	3.49 - 5.18	(4.97)	2.45 - 2.66	(2.49)	8.79 - 11.99 (11.36)	3	1.6 - 6.3	(3.3)	9.4 - 11.6	(10.6)
	Bänkerjoch Fm.	3	0.75 - 5.70	(2.85)	2.53 - 2.86	(2.71)	2.11 - 13.26 (7.41)	3	1.1 - 2.9	(2.2)	1.7 - 5.9	(5.5)
	Schinznach Fm.	4	0.50 - 7.37	(4.85)	2.44 - 2.72	(2.57)	1.34 - 16.28 (11.33)	1	1.7		0.1	
	Zeglingen Fm.	1	1.79		2.74		4.75	1	2.6		0.5	
	Kaiseraugst Fm.	2	3.18 - 4.32	(3.75)	2.59 - 2.62	(2.61)	7.91 - 10.49 (9.20)	3	2.0 - 4.8	(2.8)	7.9 - 29.7	(26.2)
	Buntsst., Permian	4	2.74 - 4.77	(3.03)	2.33 - 2.53	(2.52)	6.66 - 10.45 (7.32)	5	0.9 - 3.7	(1.4)	8.7 - 33.4	(11.3)
Nördlich Lägern (NL)	Malm	28	0.24 - 3.38	(0.65)	2.55 - 2.71	(2.65)	0.64 - 8.18 (1.72)	3	0.4 - 1.2	(0.8)	0.7 - 4.2	(0.8)
	D.A.O.	11	0.57 - 5.54	(2.84)	2.44 - 2.73	(2.57)	1.50 - 12.55 (6.98)	5	2.4 - 3.8	(2.5)	2.0 - 15.5	(11.9)
	Opalinus Clay	13	3.26 - 4.78	(4.41)	2.43 - 2.62	(2.53)	8.11 - 11.22 (10.36)	2	2.7 - 3.4	(3.0)	13.0 - 14.6	(13.8)
	Staffelegg Fm.	4	0.36 - 3.87	(2.01)	2.46 - 2.71	(2.61)	0.97 - 9.01 (4.91)	n.a.	n.a.		n.a.	
	Klettgau Fm.	7	3.62 - 6.41	(4.26)	2.40 - 2.61	(2.57)	8.80 - 14.10 (10.38)	2	1.9 - 3.1	(2.5)	7.5 - 10.2	(8.9)
	Bänkerjoch Fm.	5	0.06 - 4.27	(1.96)	2.57 - 2.88	(2.70)	0.19 - 10.28 (5.03)	2	2.2 - 3.0	(2.6)	4.6 - 11.1	(7.9)
	Schinznach Fm.	6	0.39 - 7.49	(2.26)	2.44 - 2.71	(2.67)	1.04 - 16.48 (5.85)	1	2.9		0.3	
	Zeglingen Fm.	2	0.08 - 0.15	(0.12)	2.25 - 2.91	(2.58)	0.25 - 0.35 (0.30)	1	0.5		0.6	
	Kaiseraugst Fm.	1	2.67		2.66		6.81	1	3.5		10.5	
	Buntsst., Permian	2	3.93 - 5.04	(4.48)	2.53 - 2.55	(2.54)	9.44 - 11.84 (10.64)	2	1.5 - 3.2	(2.4)	2.2 - 17.5	(9.9)
Zürich Nordost (ZNO)	Malm	13	0.45 - 4.12	(1.21)	2.54 - 2.70	(2.64)	1.19 - 9.92 (3.71)	n.a.	n.a.		n.a.	
	D.A.O.	15	2.05 - 6.97	(4.74)	2.48 - 2.62	(2.53)	5.15 - 15.82 (10.77)	4	1.5 - 2.9	(1.9)	5.8 - 14.4	(7.4)
	Opalinus Clay	17	3.77 - 5.36	(4.56)	2.47 - 2.55	(2.52)	8.99 - 12.28 (10.68)	2	3.0 - 3.1	(3.1)	13.2 - 14.6	(13.9)
	Staffelegg Fm.	7	2.65 - 5.50	(4.61)	2.36 - 2.55	(2.50)	6.32 - 12.50 (10.66)	1	3.1		14.5	
	Klettgau Fm.	6	3.75 - 7.29	(5.04)	2.38 - 2.57	(2.53)	10.94 -13.46 (11.86)	3	2.8 - 3.5	(3.5)	9.6 - 11.8	(11.1)
	Bänkerjoch Fm.	8	1.52 - 4.78	(2.56)	2.55 - 2.75	(2.66)	4.07 - 11.55 (6.50)	3	1.4 - 4.1	(3.0)	2.5 - 10.5	(8.0)
	Schinznach Fm.	8	0.22 - 6.21	(2.30)	2.53 - 2.76	(2.64)	0.56 - 14.36 (5.78)	1	1.9		0.8	
	Zeglingen Fm.	4	0.31 - 7.85	(2.70)	2.46 - 2.90	(2.69)	0.87 - 17.32 (6.46)	1	0.9		0.9	
	Kaiseraugst Fm.	2	1.66 - 3.99	(2.82)	2.60 - 2.62	(2.61)	4.23 - 9.75 (6.99)	3	2.9 - 7.2	(3.6)	9.0 - 20.5	(12.9)
	Buntsst., Permian	1	2.90		2.52		6.99	4	1.7 - 2.6	(2.5)	3.8 - 12.3	(8.1)

g_{pw}). In the Keuper aquifer (Klettgau Fm.), a tentative excursion towards lower $^4He_{pw}$ values seems indicated, while a positive excursion up to $^4He_{pw}$ values of 4.4×10^{-3} cm^3(STP)/g_{pw} is observed in the underlying Bänkerjoch Formation. As no groundwater could be collected from the Keuper aquifer in this borehole, it is not possible to directly link either of these potential excursions to a potential water-conducting zone. The δ^2H data (Gimmi et al., 2023) show a comparable profile shape in that section, with a negative excursion in the Keuper aquifer (Klettgau Fm.), which then reverts back to the general – albeit less well defined - trend with depth in the Bänkerjoch Formation. In either case, both tracers indicate diffusion controlled gradients in direction of the Muschelkalk groundwater in the Schinznach Formation with a $^4He_{gw}$ concentration of 1.3×10^{-4} cm^3(STP)/g_{gw}) and a porewater helium concentration of 6.4×10^{-4} cm^3(STP)/g_{pw} in a sample taken at 848.9 m, directly above the depth interval where the groundwater was localised (Fig. 3).

Below the Muschelkalk groundwater, the helium concentrations in the porewater gradually rise across the evaporitic and clayey Zeglingen Formation to an again relatively flat profile in the Kaiseraugst Formation and below, with $^4He_{pw}$ concentrations between 4.6×10^{-3} to 6.1×10^{-3} cm^3(STP)/g_{pw}, which represent the highest values encountered in Jura Ost.

$^3He/^4He$ signatures in the porewater have rather constant values between 2.7×10^{-7} to 3.1×10^{-7} (0.20–0.23 R_A) from the Malm to the Opalinus Clay. Near the depth of the observed excursions in the $^4He_{pw}$ and δ^2H profiles in the Keuper aquifer (around 710 m, Klettgau Fm.), higher values of 4.8×10^{-7} and 3.7×10^{-7} (0.36–0.28 R_A) are recorded, which could indicate a small contribution of an air-derived helium component via a potential Keuper groundwater. In the Muschelkalk and below, the $^3He/^4He$ porewater signatures shift to values just above 1.0×10^{-7}, (0.07 R_A), identical to the value measured in the Muschelkalk groundwater. These lower values, together with the observed increase in $^4He_{pw}$ concentrations with depth below the Muschelkalk groundwater, suggest the addition of a small fraction of a more radiogenic helium component to these porewaters potentially from below.

In BOZ2-1, groundwater was encountered in the Hauptrogenstein and Keuper aquifers (D.A.O. and Klettgau Fm., respectively) in addition to the Muschelkalk aquifer (Schinznach Fm.). While the porewater helium concentration also features a flat profile in the Opalinus Clay with $^4He_{pw}$ values closely around 2.0×10^{-3} cm^3(STP)/g_{pw}, clear, diffusion controlled profile shapes towards lower values in the bounding aquifers can be observed above and below. Similar to BOZ1-1, the $^4He_{pw}$ values measured in the aquifer intervals are significantly higher compared to the measured groundwater helium concentrations (Fig. 3). As in BOZ1-1, the porewater helium concentration profile shape matches that of the δ^2H porewater profile across the Lias-Dogger section.

Table 2
Porewater helium data, in-situ production and accumulation data summary data ranges and median values (in parentheses) of analysed samples per study area and stratigraphic unit.

		porewater helium data				in-situ production and accumulation data		
	Stratigraphy	n [-]	$^4He_{pw}$ [$cm^3(STP)_{^4He}\ g_{pw}^{-1}$]	$(^3He/^4He)_{pw}$ [-]	[R/R_A]	n [-]	$^4He_{prod}$ [$cm^3(STP)_{^4He}\ g_{rock}^{-1}\ yr^{-1}$]	$^4He_{acc}$ [$cm^3(STP)_{^4He}\ g_{pw}^{-1}\ yr^{-1}$]
Jura Ost (JO)	Malm	6 | 1	1.38E-03 - 2.66E-03 (1.59E-03)	2.78E-07	0.207	n.a.	n.a.	n.a.
	D.A.O.	7 | 1	1.11E-03 - 2.13E-03 (1.82E-03)	2.94E-07	0.219	5	3.50E-13 - 7.63E-13 (5.77E-13)	4.39E-12 - 1.88E-11 (1.44E-11)
	Opalinus Clay	9 | 1	1.64E-03 - 2.22E-03 (1.91E-03)	3.14E-07	0.234	1	7.56E-13	1.66E-11
	Staffelegg Fm.	3 | 0	7.64E-04 - 2.33E-03 (2.28E-03)	n.a.	n.a.	1	6.96E-13	1.33E-11
	Klettgau Fm.	4 | 1	3.43E-04 - 1.80E-03 (9.91E-04)	4.81E-07	0.359	3	5.04E-13 - 1.04E-12 (7.63E-13)	7.74E-12 - 2.12E-11 (1.15E-11)
	Bänkerjoch Fm.	4 | 1	1.73E-03 - 4.40E-03 (3.38E-03)	3.72E-07	0.278	3	1.84E-13 - 5.26E-13 (3.80E-13)	1.66E-12 - 1.15E-11 (3.41E-12)
	Schinznach Fm.	2 | 1	6.41E-04 - 1.29E-03 (9.67E-04)	1.29E-07	0.096	1	2.11E-13	2.37E-12
	Zeglingen Fm.	1 | 1	2.79E-03	1.17E-07	0.087	1	3.32E-13	6.32E-12
	Kaiseraugst Fm.	2 | 1	4.58E-03 - 6.14E-03 (4.58E-03)	1.15E-07	0.086	3	4.74E-13 - 1.35E-12 (1.20E-12)	1.07E-11 - 3.70E-11 (1.81E-11)
	Buntsandstein, Permian	1 | 1	5.66E-03 - 5.66E-03 (5.66E-03)	1.08E-07	0.081	5	4.44E-13 - 1.42E-12 (6.81E-13)	8.40E-12 - 2.33E-11 (1.25E-11)
Nördlich Lägern (NL)	Malm	14 | 7	1.18E-03 - 6.95E-03 (4.08E-03)	7.77E-08 - 7.02E-07 (1.56E-07)	0.116	3	6.93E-14 - 2.69E-13 (1.21E-13)	9.77E-12 - 1.73E-11 (1.70E-11)
	D.A.O.	5 | 1	1.70E-03 - 3.03E-03 (2.06E-03)	1.47E-07	0.110	5	3.64E-13 - 9.15E-13 (6.39E-13)	1.07E-11 - 2.40E-11 (1.21E-11)
	Opalinus Clay	5 | 2	2.15E-03 - 4.52E-03 (2.18E-03)	1.45E-07 - 1.99E-07 (1.72E-07)	0.128	2	7.08E-13 - 8.40E-13 (7.74E-13)	1.43E-11 - 1.47E-11 (1.45E-11)
	Staffelegg Fm.	2 | 0	2.64E-03 - 6.51E-03 (4.58E-03)	n.a.	n.a.	n.a.	n.a.	n.a.
	Klettgau Fm.	5 | 2	1.81E-03 - 2.34E-03 (2.00E-03)	1.82E-07 - 2.88E-07 (2.35E-07)	0.175	2	4.50E-13 - 6.76E-13 (5.63E-13)	6.84E-12 - 1.41E-11 (1.05E-11)
	Bänkerjoch Fm.	3 | 1	1.57E-03 - 2.20E-03 (1.83E-03)	1.48E-07	0.110	2	4.03E-13 - 6.90E-13 (5.46E-13)	4.24E-12 - 8.85E-12 (6.54E-12)
	Schinznach Fm.	3 | 2	2.32E-05 - 8.03E-04 (5.06E-04)	2.48E-07 - 2.75E-07 (2.61E-07)	0.195	1	3.63E-13	9.98E-12
	Zeglingen Fm.	2 | 1	9.87E-03 - 4.80E-02 (2.90E-02)	2.41E-07	0.180	1	7.86E-14	4.20E-11
	Kaiseraugst Fm.	1 | 1	1.18E-02	1.02E-07	0.076	1	7.33E-13	2.41E-11
	Buntsandstein, Permian	2 | 1	6.09E-03 - 8.11E-03 (7.10E-03)	9.50E-08	0.071	2	2.47E-13 - 9.00E-13 (5.74E-13)	1.40E-11 - 4.13E-11 (2.76E-11)
Zürich Nordost (ZNO)	Malm	8 | 4	2.11E-03 - 7.55E-03 (3.26E-03)	8.29E-08 - 2.91E-07 (1.89E-07)	0.141	n.a.	n.a.	n.a.
	D.A.O.	4 | 1	1.93E-03 - 3.74E-03 (2.37E-03)	2.99E-07	0.223	4	3.52E-13 - 7.73E-13 (4.40E-13)	6.37E-12 - 1.37E-11 (8.73E-12)
	Opalinus Clay	9 | 2	1.77E-03 - 3.01E-03 (2.22E-03)	3.16E-07 - 3.42E-07 (3.29E-07)	0.246	2	7.51E-13 - 8.04E-13 (7.77E-13)	1.32E-11 - 1.56E-11 (1.44E-11)
	Staffelegg Fm.	4 | 1	1.22E-03 - 4.27E-03 (1.69E-03)	3.26E-07	0.243	1	8.01E-13 - 8.01E-13 (8.01E-13)	1.48E-11 - 1.48E-11 (1.48E-11)
	Klettgau Fm.	5 | 2	9.11E-04 - 1.78E-03 (1.30E-03)	3.29E-07 - 3.81E-07 (3.55E-07)	0.265	3	6.85E-13 - 7.51E-13 (7.07E-13)	1.03E-11 - 1.19E-11 (1.11E-11)
	Bänkerjoch Fm.	5 | 1	1.02E-03 - 3.75E-03 (1.33E-03)	3.16E-07	0.236	3	2.44E-13 - 7.34E-13 (6.72E-13)	1.56E-12 - 1.28E-11 (9.10E-12)
	Schinznach Fm.	4 | 1	2.07E-05 - 4.21E-05 (3.14E-05)	4.20E-07	0.313	1	2.56E-13 - 2.56E-13 (2.56E-13)	1.16E-11 - 1.16E-11 (1.16E-11)
	Zeglingen Fm.	3 | 2	1.73E-05 - 3.07E-03 (1.58E-03)	2.92E-07 - 6.20E-07 (4.56E-07)	0.340	1	1.36E-13 - 1.36E-13 (1.36E-13)	5.03E-12 - 5.03E-12 (5.03E-12)
	Kaiseraugst Fm.	2 | 1	1.34E-03 - 1.47E-03 (1.40E-03)	1.19E-07	0.089	3	6.16E-13 - 1.48E-12 (8.15E-13)	1.60E-11 - 8.09E-11 (2.24E-11)
	Buntsandstein, Permian	n.a.	n.a.	n.a.	n.a.	4	3.59E-13 - 6.76E-13 (5.21E-13)	1.86E-11 - 2.00E-11 (1.93E-11)

4.3.2. *Study area Nördlich Lägern (NL)*

Both investigated boreholes, BUL1-1 and STA3-1 show a flat $^4He_{pw}$ profile over more than 300 m between the lower part of the Malm (625 m in STA3-1, 750 m in BUL1-1) and the Bänkerjoch Formation (Fig. 4). In STA3-1, $^4He_{pw}$ values are centered narrowly around 2.0×10^{-3} $cm^3(STP)/g_{pw}$ over this entire interval, while in BUL1-1 the values show a somewhat larger scatter from 1.6×10^{-3} to 3.0×10^{-3} $cm^3(STP)/g_{pw}$ around a mean value of 2.3×10^{-3} $cm^3(STP)/g_{pw}$, with two outlying higher values at 892 m and 1009 m. The upper sample was taken at the base of a Fe-Oolith bearing layer, whereas the lower sample is a marlstone with no discerning lithology and the reason for the higher $^4He_{pw}$ values is at this time unknown, although an analytical artefact can be excluded. While the δ^2H profile shows some scatter in the upper half of the D.A.O., where the reef-facies limestones of the Herrenwis unit (Fig. 2) are situated, no comparable scatter is observed in the $^4He_{pw}$ profile. In both boreholes, $^3He/^4He$ signatures range from 1×10^{-7} to 2×10^{-7} (0.07–0.15 R_A) in the Opalinus Clay up to the top of the Dogger (BUL1-1) or the base of the Malm (STA3-1).

Closer to the Malm groundwater, STA3-1 shows a shift towards higher $^4He_{pw}$ values between 3.7×10^{-3} to 6.3×10^{-3} $cm^3(STP)/g_{pw}$ while the groundwater helium concentration was measured one order of magnitude lower at 3.9×10^{-4} $cm^3(STP)/g_{gw}$. This contrasts the porewater δ^2H profile shape, which shows a linear convergence towards the groundwater value (Fig. 4). It also differs from BUL1-1, where the $^4He_{pw}$ profile similarly shows higher values in the Malm above 750 m (comparable to STA3-1), but then reverts back to $^4He_{pw}$ concentrations of 1.2×10^{-3} and 1.3×10^{-3} $cm^3(STP)/g_{pw}$ adjacent to the Malm groundwater which has a matching helium concentration of 2.1×10^{-3} $cm^3(STP)/g_{gw}$. While the Malm groundwater has a similar $^3He/^4He$ ratio in both boreholes (4.5×10^{-8} (0.03 R_A) in BUL1-1 and 7.8×10^{-8} (0.06 R_A) in STA3-1), there is a distinct difference in the profile shape of the $^3He/^4He$ porewater values near the Malm groundwater in the two boreholes. In STA3-1, the porewater $^3He/^4He$ signature gradually converges on the groundwater value, which is lower than the values in the more central section between the top of the Keuper and lowermost part of the Malm, suggesting an addition of a more radiogenic helium component via the groundwater. While diffusive exchange between the porewater and a groundwater enriched in radiogenic helium would lead to the observed profile shapes, the observed lower ^4He concentration in the groundwater relative to the porewater would – at present - hamper diffusion of helium from the groundwater into the porewater against a concentration gradient. Contrasting the $^3He/^4He$ profile in STA3-1, BUL1-1 shows a clear trend to less radiogenic porewater helium signatures from the top of the D.A.O. through the Malm towards the location of the Malm groundwater, which would be consistent with an air-saturated water or a less radiogenic, mantle-like helium component delivered via the groundwater. Both would, however, stand in contrast with the presently observed low $^3He/^4He$ groundwater value.

The porewater helium profiles of either borehole show no indication of potential groundwater in the Keuper aquifer (Klettgau Fm.), an observation that is corroborated by a similarly undisturbed and straight δ^2H profile over this section, as well as by the low hydraulic conductivity measured for this interval in both boreholes.

Near the Muschelkalk groundwater (Schinznach Fm.), BUL1-1 exhibits a sharp decrease in porewater helium concentration by two orders of magnitude from 1.8×10^{-3} $cm^3(STP)/g_{pw}$ in the lower Bänkerjoch Formation to 2.3×10^{-5} $cm^3(STP)/g_{pw}$ at the top of the Schinznach Formation over a vertical distance of less than 23 m. The low $^4He_{pw}$ concentration in the Schinznach Formation mirrors the Muschelkalk groundwater helium concentration of 2.1×10^{-5} $cm^3(STP)/g_{gw}$ sampled close below the porewater sample. This extreme gradient is similarly observed in the δ^2H values (Gimmi et al., 2023). In principle, this can be

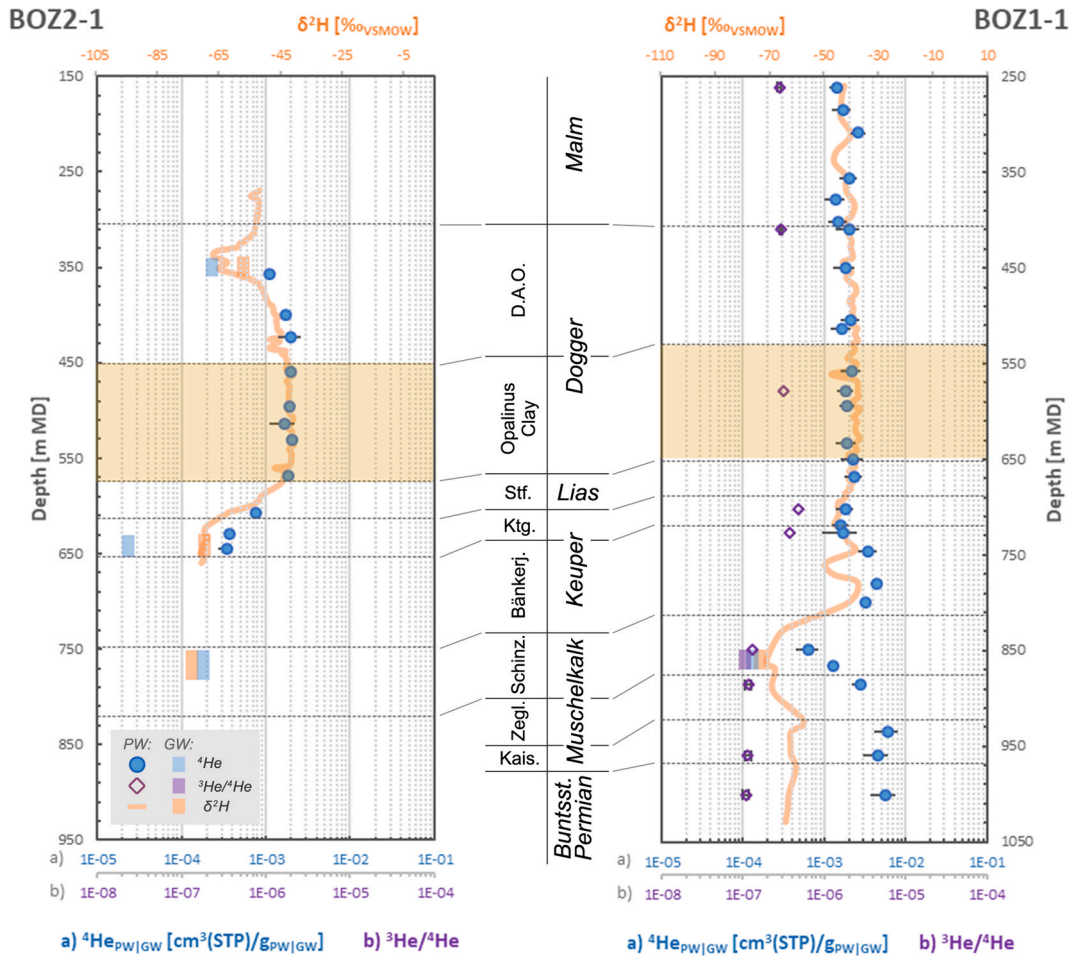

Fig. 3. Profile of ^{4}He concentrations and ^{3}He/^{4}He ratios in porewater and groundwater for boreholes BOZ2-1 (left, no ^{3}He/^{4}He data) and BOZ1-1 (right). δ^2H values (orange; Gimmi et al., 2023) are scaled in both plots to superimpose the $^4He_{pw}$ values across the Lias-Dogger sequence. The Opalinus Clay is highlighted in light umbra. D.A.O. = Dogger above Opalinus Clay; Stf. = Staffelegg Fm.; Ktg. = Klettgau Fm.; Bänkerj. = Bänkerjoch Fm.; Schinz. = Schinznach Fm.; Zegl. = Zeglingen Fm.; Kais. = Kaiseraugst Fm.; Buntsst. = Buntsandstein.

explained either by a geologically recent change in the groundwater composition and/or by extremely low diffusion coefficients in this section. The latter appears more plausible, given the fact that anhydrite-rich lithologies occur in this section (see also 5.1.2). STA3-1 also has a low helium concentration of 4.0×10^{-5} cm^3(STP)/g$_{gw}$ in the Muschelkalk groundwater, but while the porewater helium concentrations near the groundwater are significantly lower than in the overlying Bänkerjoch Formation, they remain over an order of magnitude above the groundwater value (5.0×10^{-4} and 8.0×10^{-4} cm^3(STP)/g$_{pw}$, measured on two porewater samples within the pack-off interval for the groundwater sampling). While there is no porewater helium data between 988 m and 1051 m for STA3-1, the available δ^2H data shows a less steep gradient close to the Muschelkalk aquifer compared to BUL1-1, potentially due to higher diffusion coefficients (Gimmi et al., 2023). This would then also account for the elevated porewater helium concentrations relative to the groundwater, contrasting the more strongly decoupled situation in BUL1-1. For both boreholes, ^{3}He/^{4}He values in the porewater of the lower aquitard roughly trend towards the Muschelkalk groundwater values.

Below the Muschelkalk aquifer, $^4He_{pw}$ values in STA3-1 rise again rapidly and seem to follow a positive excursion with a maximum $^4He_{pw}$ value of 4.8×10^{-2} cm^3(STP)/g$_{pw}$ in a thick halite bed overlying a sulfate rich layer at the base of the Zeglingen Formation. Below that, $^4He_{pw}$ concentrations rebound to still very high values between 6.1×10^{-3} to 8.1×10^{-3} cm^3(STP)/g$_{pw}$ in the Buntsandstein and Permian. At the same time, ^{3}He/^{4}He porewater signatures trend to apparently stable, more radiogenic values at the base of the Muschelkalk and below. These observations could be interpreted as a contribution of a more radiogenic helium component from the basement (Permian and Crystalline Basement).

4.3.3. *Study area Zürich Nordost (ZNO)*

Both investigated boreholes, MAR1-1 and TRU1-1, show a generally flat profile over the Lias-Dogger section, with $^4He_{pw}$ values in the Opalinus Clay mostly between 2×10^{-3} to 3×10^{-3} cm^3(STP)/g$_{pw}$, again very similar to the corresponding values in Jura Ost and Nördlich Lägern.

In MAR1-1, the $^4He_{pw}$ profile suggests a linear trend towards slightly lower values with depth between the top of the cored section in the Malm and the Bänkerjoch Formation, mimicking a similar general trend in the δ^2H profile (Fig. 5). At the base of the anhydrite-rich Bänkerjoch Formation, the $^4He_{pw}$ profile shows a sharp concentration drop of two orders of magnitude over no more than 30 m towards values in the range of 2-4 $\times 10^{-5}$ cm^3(STP) close to the Muschelkalk aquifer (Schinznach Fm.). Below that, in the anhydrite bearing Zeglingen Formation, the $^4He_{pw}$ concentrations return to values similar to those observed above the Muschelkalk aquifer. This behaviour is again mirrored in the δ^2H profile. Comparing the ^{4}He concentration of the Muschelkalk groundwater (1.1×10^{-6} cm^3(STP)/g$_{gw}$) with the porewater at the same location, the latter has over an order of magnitude higher concentrations – comparable to similar observations in STA3-1 and BOZ2-1 (and BOZ1-1 to a lesser degree). No Keuper groundwater was encountered in MAR1-1 and while the δ^2H profile shows a slight excursion to more negative

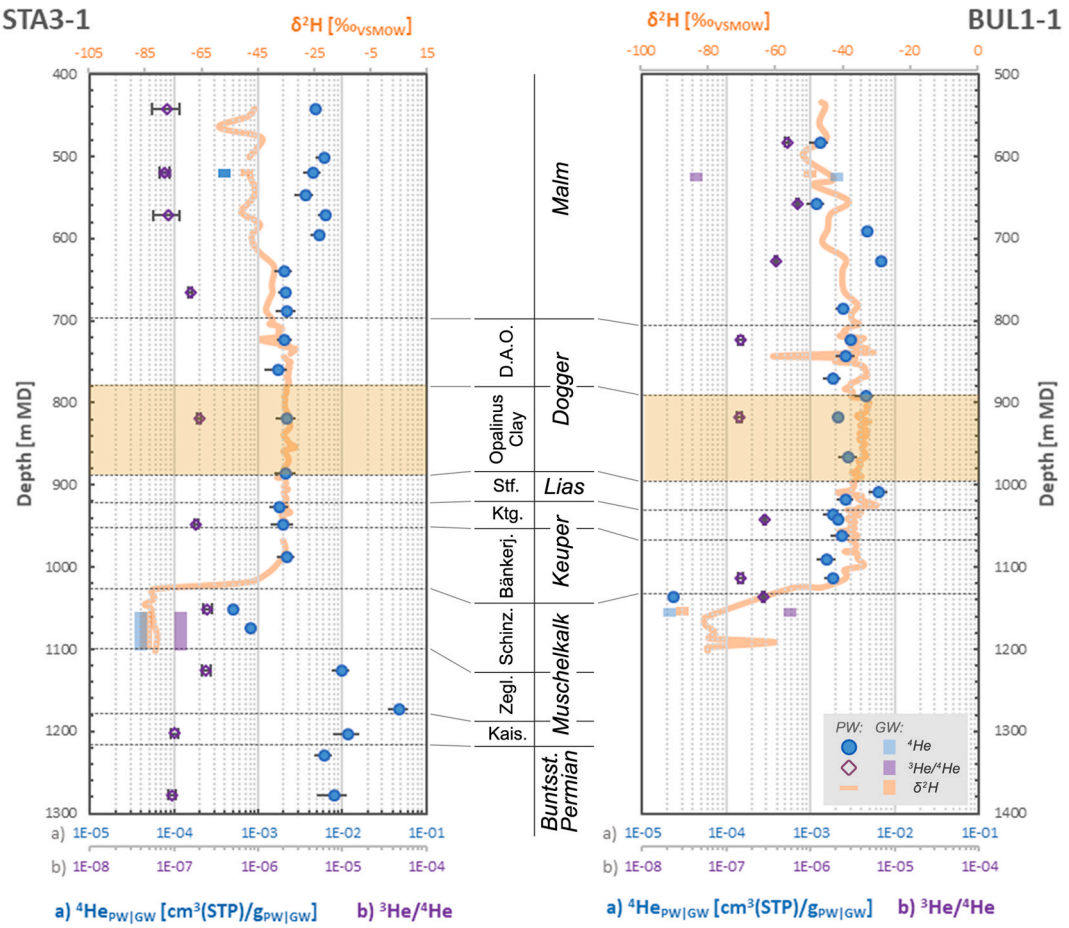

Fig. 4. Profile of ^{4}He concentrations and ^{3}He/^{4}He ratios in porewater and groundwater for boreholes STA3-1 (left) and BUL1-1 (right). δ^2H values (orange; Gimmi et al., 2023) are scaled in both plots to superimpose the $^4He_{pw}$ values across the Lias-Dogger sequence. The Opalinus Clay is highlighted in light umbra. D.A.O. = Dogger above Opalinus Clay; Stf. = Staffelegg Fm.; Ktg. = Klettgau Fm.; Bänkerj. = Bänkerjoch Fm.; Schinz. = Schinznach Fm.; Zegl. = Zeglingen Fm.; Kais. = Kaiseraugst Fm.; Buntsst. = Buntsandstein. For STA3-1 the location of the groundwater inflow in the Schinznach Formation is debated, the figure shows the entire pack-off interval. The symbols for ground- and porewater ^{3}He/^{4}He values in the Malm of STA3-1 overlap.

values in the Keuper aquifer (Klettgau Fm.), there is no clear indication of a similar behaviour in the $^4He_{pw}$ data. The ^{3}He/^{4}He porewater signatures show a very flat profile with depth, with only minor variations between 2.9×10^{-7} to 3.4×10^{-7} (0.22–0.25 R_A) over almost 400 m depth. In the Muschelkalk aquifer, the helium isotope ratios of the ground- and porewater coincide, before the latter show a trend towards increasingly more radiogenic values with depth in the anhydrite bearing Zeglingen Formation and below, with the lowermost sample at the base of the Kaiseraugst Formation measured at 1.2×10^{-7} (0.09 R_A). As in STA3-1 and BOZ1-1, such a trend could be interpreted as a contribution of a more radiogenic helium component from the basement.

In TRU1-1, the $^4He_{pw}$ profile is vertical over the Dogger but curves towards slightly lower values at the depth of the Keuper groundwater (Klettgau Fm.). In the Malm, the profile trends to elevated $^4He_{pw}$ values, while at the same time showing a more pronounced scatter compared to two underlying units. While the shape of the lower part of the helium profile is comparable to the δ^2H profile, the two clearly deviate in the Malm. The most prominent and interesting feature of the TRU1-1 profile, however, is the observation that for both the Malm and the Keuper aquifer the groundwater helium concentration clearly exceeds those of the porewater at the same depth by roughly a factor of 10. In the Malm, the $^4He_{pw}$ profile trend towards the higher groundwater value seems real, although based on a limited number of samples. In the Keuper the $^4He_{pw}$ profile stands in contradiction to the observed higher groundwater concentration, but rather seems to tentatively indicate a trend towards lower concentrations from the lowermost Lias to the Klettgau Formation. While no ^{3}He/^{4}He porewater data is available for the Lias-Dogger section, the porewater ^{3}He/^{4}He values in the Malm seem to trend towards the radiogenic groundwater signature around or below 1×10^{-7} (0.07 R_A). In the Keuper, a single ^{3}He/^{4}He porewater measurement near the groundwater has a value of 3.8×10^{-7} (0.28 R_A) comparable to the groundwater value of 2.7×10^{-7} (0.20 R_A). A detailed discussion of the TRU1-1 profiles is given in section 5.2.

5. Discussion

5.1. Evolution of the helium porewater profiles

5.1.1. In-situ production of ^{4}He in the rock matrix and accumulation in the porewater

Based on the bulk rock U and Th concentrations, ^{4}He production rates ($^4He_{prod}$ [cm^3(STP)/(g_{rock} * yr)]) can be calculated according to the formulation given by Ballentine and Burnard (2002) as

$$^4He_{prod} = \left(\left(3.115 \times 10^6 + 1.272 \times 10^5\right) * [U] + 7.710 \times 10^5 * [Th]\right) * \frac{22711}{6.022 \times 10^{23}} \quad (5)$$

where [U] and [Th] are the respective radionuclide concentrations in the rock in mg/kg, 6.022×10^{23} is the Avogadro constant (de Bievre and Peiser, 1992) and 22711 is the molar gas volume in cm^3(STP)/mole (Mohr et al., 2016).

Most of the helium produced in the rock matrix is subsequently released to the porewater, with release coefficients (λ) depending on the

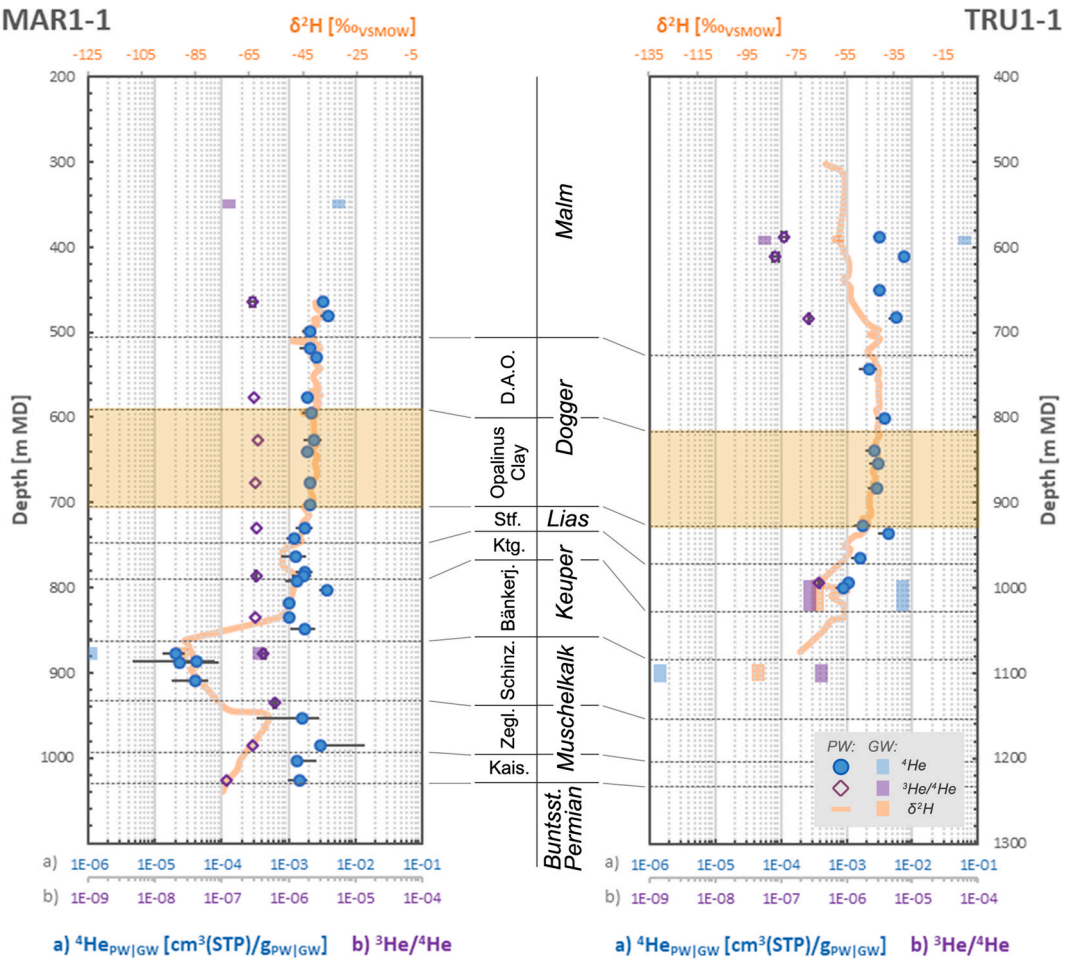

Fig. 5. Profile of ^{4}He concentrations and ^{3}He/^{4}He ratios in porewater and groundwater for boreholes MAR1-1 (left) and TRU1-1 (right). δ^2H values (orange; Gimmi et al., 2023) are scaled in both plots to superimpose the $^4He_{pw}$ values across the Lias-Dogger sequence. The Opalinus Clay is highlighted in light umbra. D.A.O. = Dogger above Opalinus Clay; Stf. = Staffelegg Fm.; Ktg. = Klettgau Fm.; Bänkerj. = Bänkerjoch Fm.; Schinz. = Schinznach Fm.; Zegl. = Zeglingen Fm.; Kais. = Kaiseraugst Fm.; Buntsst. = Buntsandstein.
Note that the ^{4}He and ^{3}He/^{4}He axes start at one decade lower than in the plots from the other areas.

texture and mineralogy of the lithology. While no helium release coefficients were determined in the TBO project, comparable data is available from Mesozoic sedimentary rocks from various boreholes such as those in Benken and Schlattingen (both NE Switzerland; Rufer and Waber, 2015; compilation in Waber and Traber 2022) or the BDB1 borehole (Mt. Terri, NW Switzerland, Rufer et al., 2018) - all of which cover the same Triassic-Jurassic aquitard sequence as the TBO boreholes. Overall, reported helium release coefficients range between 90% and 98% in clay-rich lithologies such as claystones and marl-to siltstones as well as limestones, while more sandy lithologies generally have lower values below 85%. These studies do, however, not contain helium release coefficients for anhydrite- and halite-bearing rocks. These data were therefore taken from an available data set of corresponding lithologies from the Paris Basin (Waber 2012), where strongly reduced release coefficients were reported for a halite sample (72%) and for an anhydritic dolomite sample (13%). For this study and as a first order approximation, release coefficients of 95% were assumed for relatively pure calcareous to clay-rich mineralogies (limestones, dolostones, marls, claystones); 90% for their corresponding, more sandy/silty equivalents; 85% for silt- and sandstones as well as their calcareous and argillaceous varieties. For halite and anhydrite (or samples where these minerals dominate), release coefficients of 72% and 13%, respectively, were assumed.

The helium released from the rock matrix then accumulates in the porewater at an annual rate ($^4He_{acc}$ [cm^3(STP)/(g$_{pw}$ * yr)]) of (modified from Torgersen 1980)

$$^4He_{acc} = {}^4He_{prod} * \lambda * \frac{\rho_{bulk\ wet}}{\rho_{pw}} * \frac{1-\varphi_{WL}}{\varphi_{WL}} \quad (6)$$

Calculated ^{4}He in-situ production and accumulation rates are tabulated in Table 2 as min/max ranges and median values based on the corresponding values of all samples of the respective stratigraphic unit for which these parameters could be calculated.

^{4}He production and accumulation show broadly comparable ranges over most of the stratigraphic stack for all three study areas, with the majority of the individual $^4He_{prod}$ values ranging from 4 - 8 × 10^{-13} cm^3(STP)/(g$_{rock}$ * yr and $^4He_{acc}$ between 1 and 2 × 10^{-11} cm^3(STP)/(g$_{pw}$ * yr).

Notable deviations are predominantly tied to distinctly lower ^{4}He in-situ production in the evaporites (anhydrite, halite) as well as dolo- and limestones. This is apparent in clearly lower minimum $^4He_{prod}$ values in the evaporite bearing units of the Bänkerjoch and Zeglingen formations, where such lithologies have been sampled (anhydrite in JO and ZNO, halite in NL and JO (BOZ1-1)), as well as overall lower $^4He_{prod}$ in the Malm (sampled only in NL) and the Schinznach Formation, which are dominated by limestones with low parent radionuclide concentrations.

For in-situ accumulation of helium in the porewater, however, the lower in-situ production in the above-mentioned lithotypes acts in combination with these lithologies' release coefficients as well as their porosities. For anhydrite and halite, the cumulation of low production

and low release rates can only partially be compensated by their generally low porosity, which is – among others - observed in the low overall $^4He_{acc}$ range of the Bänkerjoch Formation of JO, where the sample set consists primarily of anhydrite samples. In contrast, limestones can – despite their low production rates – efficiently enrich helium in the porewater due to their high release rate, combined with low porosities. The latter is exemplified by the accumulation values obtained for the Malm in NL, which are – despite much lower production terms – comparable to the values for the more clay-rich units such as the Opalinus Clay. It also explains why the presence of the Herrenwis Unit in the same study area has no discernible effect on the measured $^4He_{acc}$ range, similar to the observation of the undisturbed $^4He_{pw}$ profile across this unit (Fig. 4), despite two out of five samples making up the D.A.O. sample set used to calculate helium production and accumulation being from this unit. In the ZNO study area, the $^4He_{prod}$ and $^4He_{acc}$ ranges of the Lias-Dogger section correspond within ±25% to corresponding data reported from the Benken borehole by Rufer and Waber (2015) and the compilation given in Waber and Traber (2022).

5.1.2. *Minimum helium buildup times and diffusion timescales*

The minimum time (t_{min}) that would be required to produce the presently observed porewater helium inventory exclusively through in-situ production in the rock and release to the porewater, i.e. under closed system conditions (no in- and outflux from the rock-porewater system), is calculated as

$$t_{min} = \frac{^4He_{pw}}{^4He_{acc}} \quad (7)$$

The theoretical maximum accumulated ^4He in the porewater of a sample under closed conditions ($^4He_{acc\ max}$ [$cm^3(STP)/g_{pw}$]) is calculated as

$$^4He_{acc\ max} = {}^4He_{acc} * t_{sedim} \quad (8)$$

with t_{sedim} being the time since deposition of the sediment in years.

Calculated $^4He_{acc\ max}$ and t_{min} median values for the various stratigraphic units of the investigated boreholes are tabulated in Table 3.

When comparing the measured, present-day $^4He_{pw}$ concentrations of the TBO borehole profiles with the calculated total accumulated ^4He in the porewater since the time of deposition of the sediments ($^4He_{acc.\ max}$), it becomes evident that, at least in the central Lias-Dogger sequence, some of the helium produced in these units since their deposition must have been lost. This is illustrated by t_{min} durations which are below the average absolute ages of these sediments.

Contrastingly, in particular evaporite rich units below the Lias-Dogger sequence, such as the Bänkerjoch and Zeglingen formations,

Table 3
Maximal accumulated ^4He in porewater since time of deposition, minimum build-up time, diffusion parameters and diffusion timescales per study area and stratigraphic unit.

	Stratigraphy	$^4He_{acc.\ max}$ [$cm^3(STP)/g_{pw}$]	t_{min} [Ma]	$D_{eff\perp}$ (extrapol.) [$m^2\ s^{-1}$]	$D_{eff\perp}$ (meas.) [$m^2\ s^{-1}$]	L [m]	t_D (extrapol.) [Ma]	t_D (meas.) [Ma]
Jura Ost (JO)	Malm	n.a.	n.a.	3.0E-11	3.4E-11	309	4.55	3.97
	D.A.O.	2.44E-03	133	4.0E-11	4.6E-11	124	0.65	0.57
	Opalinus Clay	2.88E-03	115	2.9E-11	2.4E-11	121	0.96	1.16
	Staffelegg Fm.	2.43E-03	178	3.5E-11	3.4E-11	37	0.07	0.08
	Klettgau Fm.	2.63E-03	145	3.8E-11	4.8E-11	31	0.05	0.04
	Bänkerjoch Fm.	8.10E-04	*990*	4.9E-12	4.8E-11	93	2.25	0.23
	Schinznach Fm.	5.71E-04	*409*	6.9E-12	n.a.	63	1.02	n.a.
	Zeglingen Fm.	1.54E-03	*441*	3.0E-12	n.a.	46	0.55	n.a.
	Kaiseraugst Fm.	4.46E-03	*295*	1.8E-11	n.a.	45	0.18	n.a.
	Buntsandstein, Permian	3.30E-03	*462*	3.9E-11	n.a.	70	0.18	n.a.
Nördlich Lägern (NL)	Malm	2.62E-03	*269*	1.2E-11	1.5E-11	290	4.72	3.60
	D.A.O.	2.04E-03	155	1.7E-11	2.7E-11	83	0.87	0.53
	Opalinus Clay	2.52E-03	149	2.5E-11	2.8E-11	109	0.86	0.75
	Staffelegg Fm.	n.a.	n.a.	1.6E-11	1.6E-11	35	0.09	0.09
	Klettgau Fm.	2.35E-03	180	4.2E-11	6.1E-11	29	0.04	0.03
	Bänkerjoch Fm.	1.56E-03	*335*	1.1E-11	n.a.	75	0.15	n.a.
	Schinznach Fm.	2.42E-03	65	2.8E-11	n.a.	73	0.15	n.a.
	Zeglingen Fm.	1.02E-02	*688*	n.a.	n.a.	79	n.a.	n.a.
	Kaiseraugst Fm.	5.92E-03	*489*	n.a.	n.a.	37	n.a.	n.a.
	Buntsandstein, Permian	7.14E-03	268	n.a.	n.a.	65	n.a.	n.a.
Zürich Nordost (ZNO)	Malm	n.a.	n.a.	2.7E-11	4.6E-12	248	1.62	9.51
	D.A.O.	1.47E-03	*237*	3.7E-11	4.3E-11	88	0.40	0.34
	Opalinus Clay	2.50E-03	149	2.5E-11	2.7E-11	115	1.02	0.93
	Staffelegg Fm.	2.81E-03	100	2.9E-11	1.6E-11	42	0.11	0.20
	Klettgau Fm.	2.53E-03	148	2.2E-11	4.4E-11	42	0.17	0.08
	Bänkerjoch Fm.	2.15E-03	147	5.8E-12	n.a.	72	1.14	n.a.
	Schinznach Fm.	2.79E-03	3	1.1E-11	n.a.	70	0.52	n.a.
	Zeglingen Fm.	1.22E-03	*462*	3.2E-12	n.a.	62	3.56	n.a.
	Kaiseraugst Fm.	5.49E-03	63	2.3E-11	n.a.	36	0.26	n.a.
	Buntsandstein, Permian	5.20E-03	n.a.	n.a.	n.a.	64	n.a.	n.a.

often have $^4He_{pw}$ concentrations exceeding their $^4He_{acc.\ max}$ values, consequentially resulting in t_{min} durations often well above the average numeric age of the units. This confirms, as expected, that the porewater of these aquifer-aquitard stacks must be considered an open system with respect to diffusive gas transport. In these systems, in-situ produced helium is diffusively redistributed along the concentration gradient, generally from the units of the central Lias-Dogger sequence with high in-situ production and accumulation rates towards the over- and underlying units and finally into the bounding groundwaters with significantly lower helium concentration. This transient diffusive influx of ^4He into rock units with often lower ^4He in-situ production therefore leads to apparently "excess" $^4He_{pw}$ relative to the lithology's in-situ ^4He production potential. This is exacerbated in lithologies containing anhydrite or halite (e.g. in the Bänkerjoch and Zeglingen formations), which have low porosities and act as diffusive barriers. In situations where the concentration gradient is reversed – with helium concentrations in the bounding groundwater being so high that they exceed those in the aquitard – the (now reversed) diffusive redistribution of helium also leads to "excess" $^4He_{pw}$ in low porosity units and may in some cases even lead to "excess" $^4He_{pw}$ and overestimated t_{min} in units with moderately high in-situ production and accumulation, such as e.g. in the D.A.O. of boreholes MAR1-1 and TRU1-1 (ZNO), which both have Malm groundwater helium concentrations much higher than the porewaters in their Lias-Dogger sequences.

A comprehensive numerical model for in-situ production and diffusive-transport of He in the given geological and hydrogeochemical framework of the investigated boreholes is beyond the scope of this study. It is, however, possible to roughly gauge whether the observed porewater helium profiles are well established and potentially close to steady-state or still in a rather young, transient state by calculating diffusion timescales t_D for diffusive transport of helium across the various stratigraphic units. These timescales represent the average time required for an atom of a given element to cross that entire stratigraphic unit along a one-dimensional path by diffusion in the porewater and are calculated as

$$t_D = \frac{L^2}{2 * \frac{D_{eff\perp}}{\varepsilon}} \tag{9}$$

where L is the length of the diffusive transport (in this case the thickness of the stratigraphic section), $D_{eff\perp}$ is the effective diffusion coefficient perpendicular to bedding and ε is the diffusion accessible porosity ($D_{eff\perp}/\varepsilon$ equals the pore diffusion coefficient $D_{p\perp}$ perpendicular to bedding). For species such as noble gases or HTO (tritiated water) that are unaffected by retardation or ion exclusion, ε can be accurately approximated by the water loss porosity ($\Phi_{WL\ wet}$).

For lithologies similar to those encountered in the investigated boreholes, only a limited number of experimentally determined *helium* diffusion coefficients are available, covering exclusively clay-rich lithologies (e.g. Jacops et al., 2017). For HTO, diffusion coefficients for the encountered aquitard lithologies are reported in the literature, from Mont Terri (for a discussion see Rufer et al., 2018) as well as from NE Switzerland, both from existing boreholes (Van Loon, 2014) and measured in the context of the TBO campaign (Van Loon et al., 2023). As these analyses primarily cover the stratigraphic sequence between the Malm and the Klettgau Formation, there is still a scarcity of D_{eff} data in the stratigraphic units of the Bänkerjoch Formation and below. To complement the measured diffusion coefficients, Gimmi et al. (2023) formulated a method to extrapolate D_{eff} values for HTO as a function of clay content, using the available measured values as calibration points. In the present study, these calculated diffusion coefficients, which have a vertical resolution of approximately one value per 3–6 m, are used for stratigraphic units where insufficient measured values are available. To obtain D_{eff} values for helium, the HTO diffusion coefficients are scaled by multiplication with the ratio of the free water diffusion coefficients of helium and HTO ($D_{0(He)}/D_{0(HTO)} = 3.17$; Cook and Herczeg, 2000). All measured or extrapolated D_{eff} values are perpendicular to bedding ($D_{eff\perp}$) and the harmonic means of all available values per stratigraphic unit used in this study for the calculation of diffusion timescales are tabulated in Table 3.

In general, the harmonic means of measured and extrapolated $D_{eff\perp}$ are in good agreement for most stratigraphic units in all three study areas. The two exceptions to this are the higher and lower harmonic means of the measured compared to the extrapolated values in the Bänkerjoch Formation of JO and the Malm in ZNO, respectively. In both cases, the limited number of measured samples insufficiently represents the range of lithologies present in these units (underrepresenting anhydrite rich section in JO and more clay rich sections in ZNO).

For the homogeneous Opalinus Clay, both measured and extrapolated $D_{eff\perp}$ values are near identical in all three study areas, underlining this unit's low lateral variability in terms of lithology (see also Mazurek et al., 2023). The evaporitic sediments of the Bänkerjoch and Zeglingen formations generally have distinctly lower $D_{eff\perp}$ values compared to the stratigraphic units directly adjacent to them, which coincides with the observation of pronounced $^4He_{pw}$ concentration gradients in these units. The rather discrete localisation of these gradients – often near the bottom of the Bänkerjoch Formation (MAR1-1, STA3-1, BUL1-1) or the top of the Zeglingen Formation (MAR1-1, STA3-1) suggests that the diffusive barrier is potentially comprised of (a) singular low-diffusivity layer(s) more than being a cumulative effect over an entire section comprised of multiple such layers with varying thickness. The barrier function of evaporite layers with respect to noble gas migration was also proposed based on noble gas observations made in other sedimentary basins on groundwater above and below such layers (e.g. Tyne et al., 2022).

Diffusion timescales t_D could be calculated for at least the entire stratigraphic stack between the Malm and the Muschelkalk aquifer and are tabulated in Table 3. Values of t_D much lower than the calculated t_{min} for the respective units can be interpreted as indicative that the system would approach steady state conditions over t_{min} when assuming only slowly changing boundary conditions. For all units across all areas, calculated t_D values range at or (mostly) below 1 Ma, with exception of higher values in some of the evaporitic units (2.25 and 1.14 Ma in the Bänkerjoch Formation of JO and ZNO and 3.56 Ma in the Zeglingen Formation of ZNO) due to their low diffusivity for helium. The Malm has values broadly between 1 and 5 Ma, primarily due to its greater thickness. As the minimum times required to build up the presently observed $^4He_{pw}$ inventories in the individual stratigraphic units are much longer than the corresponding t_D, the porewater helium system should reach near steady-state conditions over these times when assuming only slowly changing boundary conditions. This, together with the observed flat $^4He_{pw}$ profiles in the clay-rich central sections, implies that the $^4He_{pw}$ inventory across the Lias-Dogger aquitard is the result of a long-term evolution of the porewater system. The observed curvatures of the profiles near the bounding aquifers, as well as the presence of helium in excess to the in-situ production in many of the stratigraphic units bounding the Lias-Dogger sequence, is evidence that the porewater helium system is primarily transport-rather than in-situ production controlled.

5.2. Porewater – groundwater helium exchange

In all aquifers, compositions and evolution of groundwater collected from the different boreholes are in line with those obtained during investigations preceding the TBO programme. Groundwater residence times were determined based on ^{14}C, ^3H and ^{39}Ar measurements and stable isotope signatures (Waber and Traber, 2022 and references therein) as well as more recently using ^{81}Kr dating (Waber et al., 2023 and references therein).

Malm groundwaters represent mixtures of a Tertiary marine to marine-brackish component and (a) dilute meteoric component(s) of warm-climate origin that infiltrated during early to middle Pleistocene times based on the groundwater chemistry and isotope signatures

(Waber and Traber 2022 and references therein). In these groundwaters, ^{4}He concentration vary between 3.92 × 10^{-4} to 6.30 × 10^{-2} $cm^3(STP)/g_{gw}$ in the investigated boreholes (Figs. 4 and 5) with associated $^3He/^4He$ ratios of 4.45 × 10^{-8} to 1.29 × 10^{-7} (0.03–0.10 R_A).

Groundwater in the Keuper aquifer is of meteoric origin and infiltrated during warm-climate periods during early to middle Pleistocene times (Waber and Traber 2022 and references therein). In the investigated boreholes, the Keuper aquifer could only be sampled in BOZ2-1 with a ^{4}He concentrations of 2.33 × 10^{-5} $cm^3(STP)/g_{gw}$ and in TRU1-1 with a ^{4}He concentration of 7.00 × 10^{-3} $cm^3(STP)/g_{gw}$ (Figs. 3 and 5). The associated $^3He/^4He$ ratios vary between 1.83 × 10^{-7} and 4.83 × 10^{-6} (0.14–0.36 R_A).

Muschelkalk groundwaters are all meteoric waters that infiltrated during the last glacial stage in the Late Pleistocene based on their chemistry and isotope signatures. In agreement with previous data (Waber and Traber 2022 and references therein), the short residence time, coupled with the generally observed high water yield, results in the Muschelkalk aquifer acting as an effective flushing pathway for the helium porewater system in the lower part of the investigated sediment stack. Consequentially, the ^{4}He concentrations in the Muschelkalk groundwaters are comparably low and generally increase from east to west. They vary between 1.09 × 10^{-6} and 4.02 × 10^{-5} $cm^3(STP)/g_{gw}$ in the investigated ZNO and NL boreholes and are almost an order of magnitude higher in the JO boreholes (Figs. 3, Fig. 4, Fig. 5). In contrast, the corresponding $^3He/^4He$ ratios show less variation between 1.06 × 10^{-7} to 5.77 × 10^{-7} (0.08–0.43 R_A).

Looking at the relation between ^{4}He concentrations and $^3He/^4He$ signatures between groundwaters and porewaters derived from nearby samples, three different scenarios can be distinguished in the bounding aquifers above and/or below the low-permeability sequences. In this context it should be recalled that the Keuper and Muschelkalk groundwaters are intercalated between over- and underlying aquitards, whereas the Malm groundwater is only exposed to the underlying aquitard of the Lias-Dogger sequence.

5.2.1. Scenario 1

The ^{4}He concentrations, which are up to more than three orders of magnitude higher in the porewater of the Lias-Dogger aquitard section compared to the groundwater, converge towards the ^{4}He concentrations of the nearest aquifers and the samples most proximal to the groundwater retain $^4He_{pw}$ concentrations approximately 6–20 times higher than the groundwater. This convergence is controlled by diffusive transport and the resulting profile shapes are strongly affected by the transport properties of the encountered lithologies, as seen in the more continuously curved profiles of JO compared to the sharp, almost discrete, and very steep gradients across low-permeability evaporite layers directly above the Muschelkalk aquifer in STA3-1, BUL1-1 and MAR1-1. In all these cases, the $^3He/^4He$ signatures of the groundwaters and the adjacent porewaters are identical (MAR1-1, BOZ1-1) or similar within a factor of two (STA3-1). This is comparable to other helium profiles reported from the Swiss Molasse basin in the literature (e.g. Nagra, 2002; Rufer and Waber, 2015; Tolstikhin et al., 1996, 2011, 2018). In all these cases, the groundwater helium inventory is predominantly supplied by the in-situ produced helium derived from the adjacent aquitards and may contain only subordinate amounts of externally sourced helium, such as a few percent of mantle-derived helium, as is ubiquitously observed in ground- and porewaters (Rufer and Waber, 2015; Waber and Traber 2022 and references therein).

5.2.2. Scenario 2

Similar to scenario 1, but with ^{4}He concentrations of the groundwater and adjacent porewater being identical within less than a factor of two. This scenario is observed only for the Malm and Muschelkalk aquifers in BUL1-1. While the latter also has similar $^3He/^4He$ ground- and porewater values, the helium isotope signatures of the Malm porewater and groundwater are very divergent, with the porewater $^3He/^4He$ ratios above the Opalinus Clay trending away rather than towards the groundwater value. Currently, we have no simple explanation to explain the relationship in the Malm, but it is likely a result of superimposed events in the Malm groundwater, whereas the relationship in the Muschelkalk could indicate a stronger addition of helium from the overlying aquitard (Bänkerjoch Fm.) compared to the flux from greater depth in agreement with the developed steep gradient in $^4He_{pw}$ directly above the aquifer.

5.2.3. Scenario 3

This scenario is observed in the TRU1-1 borehole, both at the Malm and the Keuper aquifer locations. In both cases, the groundwater ^{4}He concentration exceeds the $^4He_{pw}$ concentration of the adjacent porewater samples by roughly a factor of 10 while the $^3He/^4He$ signatures of ground- and porewaters for both aquifers are near identical (Fig. 5).

For a system to show such elevated groundwater concentrations relative to the aquitard porewater values as observed in TRU1-1 requires that the groundwater helium inventory comprises a large fraction of helium from a source external of the investigated aquitard-aquifer sequence. In the present case, this external helium cannot have been supplied to the different aquifers in the form of a helium flux from depth across the Mesozoic sediment stack, as the Muschelkalk groundwater with its very low $^4He_{gw}$ concentration would act as an effective barrier impeding a pervasive diffusive helium transport upwards against the concentration gradient. Similarly, such a vertical flux would result in $^4He_{pw}$ concentrations in the aquitard between the Keuper and Malm aquifers to be at least equal to the Keuper groundwater concentration. In consequence, the external helium must be supplied to the aquifers in a manner that largely bypasses the sediment stacks between the aquifers. Based on the groundwater chemistry, gas and isotope compositions of the groundwaters in the Malm, Keuper and Muschelkalk aquifers, Waber et al. (2023) propose a possible pathway along a steep tectonic lineament crosscutting the entire sediment stack, such as the NW-SE striking Neuhausen fault situated at a surface distance of less than 1 km to the north-east.

In such a scenario, possible sources for the high concentrations of radiogenic noble gases as well as CH_4 and CO_2 detected in the Keuper and particularly the Malm groundwater are the underlying sediments of the Permo-Carboniferous Trough (PCT) and the crystalline basement. Sediments of the PCT have an average annual ^{4}He in-situ production rate of 1.4 ± 0.7 × 10^{-12} $cm^3(STP)/(g_{rock} * a)$ as measured by Tolstikhin et al. (2011, 2018) on 7 shale and sandstone samples from the Permian section of the PCT in the Weiach deep borehole. The calculated $^3He/^4He$ production ratio for these samples is on average 5.1 ± 3.2 × 10^{-8}, (0.04 ± 0.02 R_A), with the sandstones having a more radiogenic production ratio of 1.6 × 10^{-8} (0.01 R_A). As such, these sediments have a roughly 2 to 3 times higher in-situ production of helium with a more radiogenic $^3He/^4He$ ratio than the investigated sediments of the Mesozoic cover (average $^3He/^4He$ for the Lias-Dogger sequence from Benken and Schlattingen boreholes is 3.82 × $10^{-8}R_A$), Waber and Traber, 2022). For the crystalline basement, the ^{4}He production rate of 6.5 × 10^{-13} $cm^3(STP)/(g_{rock} * a)$ is roughly comparable to the Mesozoic sediments, while its $^3He/^4He$ production ratio is even more radiogenic at 1.08 × 10^{-8} (0.01 R_A) (Ballentine and Burnard, 2002; average values for Upper Crust). Based on chemical evidence the addition to the groundwaters is limited to gases as the low mineralisation of the Muschelkalk groundwater (Cl = 26.8 mg/L) inhibits the addition via a water phase, which can be expected to be highly saline (see Waber and Traber 2022).

Enrichment of the Muschelkalk, Keuper and Malm aquifers by such a PCT or basement derived helium migrating upwards along a fault plane would to a large part be controlled by the relationship between the ascending helium flux and the groundwater flux. Aquifers with low flow rates and high residence times would become more enriched in helium and have their $^3He/^4He$ signature shifted more towards the radiogenic $^3He/^4He$ signature of the enriching component compared to faster flowing aquifers with lower residence times. With the groundwater

residence times gradually increasing from the Muschelkalk to the Keuper and Malm aquifers in ZNO, the observed groundwater concentrations and $^3He/^4He$ signatures qualitatively fit with this conceptual enrichment model (Fig. 6).

- The well flushed Muschelkalk groundwater has the lowest $^4He_{gw}$ concentration (1.4×10^{-6} $cm^3(STP)/g_{gw}$) and simultaneously the most non-radiogenic $^3He/^4He$ (4.13×10^{-7} (0.31 R_A)) of the three groundwaters, clearly trending towards an air-saturated water helium composition. This indicates that the contribution of the PCT or basement derived helium to this groundwater is not clearly detectable, potentially due to strong dilution by the high groundwater flow.
- The TRU1-1 Keuper groundwater with its intermediate residence time has the highest helium concentration (7.0×10^{-3} $cm^3(STP)/g_{gw}$) observed in any Keuper groundwater from deep boreholes in northern Switzerland so far. Relative to the adjacent porewater samples, the $^4He_{gw}$ concentration is a factor of 7 higher, which corresponds to an absolute excess $^4He_{gw}$ concentration of 5.9×10^{-3} $cm^3(STP)/g_{gw}$ compared to the porewater. The $^3He/^4He$ signature of the Keuper groundwater (2.71×10^{-7} (0.20 R_A)) is slightly more radiogenic compared to the Muschelkalk groundwater (4.13×10^{-7} (0.31 R_A)) and is congruent within a factor of 2 with the signature of an adjacent porewater sample, indicating the preservation of a certain degree of enrichment of the Keuper groundwater by the external PCT or basement derived helium component.

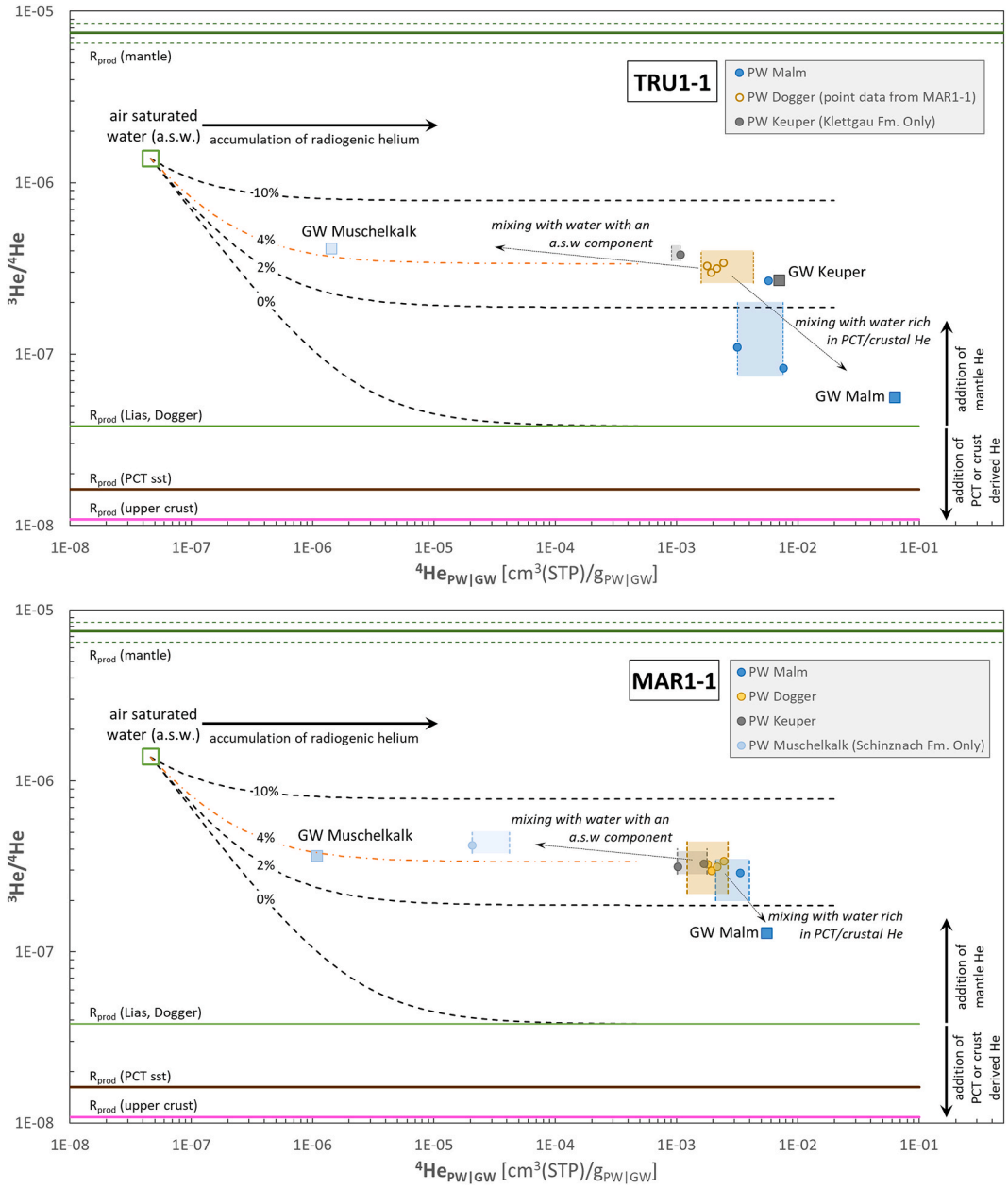

Fig. 6. Mixing relations between various helium components in the TRU1-1 (above) and MAR1-1 (below) boreholes.
The dashed lines indicate mixing lines between air saturated water (ASW; Kipfer et al., 2002) and the average in-situ produced helium from the Lias-Dogger sequence (R_{prod} (Lias, Dogger)) with increasing admixture of mantle derived helium, with the orange 4% admixture line indicating the best fit with the porewater of the main aquitard (data "PW Dogger"). Data points indicate individual porewater samples where both $^4He_{pw}$ and $^3He/^4He$ are available, shaded areas indicate range of $^4He_{pw}$ measured for this stratigraphic section. For the Dogger in TRU1-1 no porewater samples with both $^4He_{pw}$ and $^3He/^4He$ are available, the figure shows the corresponding data from MAR1-1 as proxy over the shaded $^4He_{pw}$ range from TRU1-1. For R_{prod} values, see text.

- The Malm groundwater in borehole TRU1-1 has the highest ^4He concentration (6.3×10^{-2} $cm^3(STP)/g_{gw}$) measured in any groundwater of northern Switzerland so far, combined with a radiogenic $^3He/^4He$ ratio of 5.61×10^{-8} (0.04 R_A), as the very high residence time of this groundwater allows for an extensive enrichment with the external PCT or basement helium component. The groundwater has a $^4He_{gw}$ concentration a factor 8 higher than the highest concentrated adjacent porewater sample. While this is similar to the porewater/groundwater relation in the Keuper, the absolute $^4He_{gw}$ excess in the Malm groundwater compared to the porewater is with 5.6×10^{-2} $cm^3(STP)/g_{gw}$ almost 10 times higher than in the Keuper aquifer. This is in line with the measured $^3He/^4He$ signatures of the groundwater, which trend towards more radiogenic values derived from the PCT or basement helium component. At the moment no $^3He/^4He$ porewater data is available for the Lias-Dogger sequence, but considering the lithological similarity as well as the comparable $^4He_{pw}$ values in this section of the two investigated ZNO boreholes it seems reasonable to assume $^3He/^4He$ signatures of around 3×10^{-7} (0.2 R_A) for the Dogger in TRU1-1, congruent to the values measured in MAR1-1. In this case, both the $^4He_{pw}$ concentration and the associated $^3He/^4He$ signatures above the D.A.O. trend towards the groundwater values, suggesting at least partial equilibration between the groundwater and the porewater, with helium from the groundwater diffusing into the porewater. Due to the much higher helium inventory and residence time of the Malm groundwater compared to the Keuper, the same effect is less visible in the latter. Considering the very long residence time of the Malm groundwater, it seems contradictory that the groundwater-porewater equilibration in this aquifer is only partial. It must be kept in mind, however, that the groundwater residence time only provides a temporal constraint on the presence of the *groundwater*, but not the *helium* in it. It is plausible that some younger event has triggered or facilitated a gas flow along the Neuhausen fault. This is supported by Gimmi et al. (2023) who observe a decoupling and pronounced deviation of the δ^2H and $\delta^{18}O$ profiles above 720 m (lowermost Malm), which they suggest could be indicative of a younger change to the Malm groundwater.

Looking at the MAR1-1 borehole, located approximately 6 km west-southwest of TRU1-1 and along the general groundwater flow direction for all three groundwaters, similar observations can be made (Figs. 5 and 6). The Malm groundwater (no Keuper groundwater was encountered) as well as the porewaters in the Keuper-Malm interval show the same mixing trends as those in TRU1-1, albeit to a more limited extent. The apparently reduced enrichment with the PCT or basement derived helium component in MAR1-1 relative to TRU1-1, particularly clearly observable in its much lower influence on the Malm groundwater, is explained by the almost stagnant state of the Malm groundwater, in which the external helium component propagates primarily through (slow) diffusion. This, coupled with the constant diffusive loss of helium from the groundwater into the lower concentrated porewater along its path results in the observed attenuation.

In order to verify this conceptual model and to constrain the evolution of these ground- and porewaters quantitatively and temporally, additional data as well as a comprehensive, numerical helium production and transport model is required and is planned for the foreseeable future.

6. Conclusions and outlook

The presented, expansive and highly resolved dataset of porewater helium data provides a basis to investigate porewater and groundwater evolution across the entire Jurassic-Triassic aquitard sequence of NE-CH on a large vertical and lateral scale. It complements similar datasets of chemical and isotope tracers acquired on the same drillcores. Over the central Lias-Dogger aquitard section, all porewater helium profiles show remarkably similar concentrations and overall flat profile shapes with depth, with the partial exception of BOZ2-1, where the upper- and lowermost parts of the profiles already show a diffusion trend in direction of the lower-concentrated bounding groundwaters. Closer to the aquifers, the $^4He_{pw}$ profile shapes indicate that the porewater helium system is controlled by diffusive transport, with specific cases (MAR1-1, BUL1-1, perhaps STA3-1) being modified by strata with very low diffusivity in the Bänkerjoch and Zeglingen formations (anhydrite, halite beds) acting as diffusive barriers and resulting in sharp steps in the $^4He_{pw}$ profiles. While there is an overall very good agreement between the $^4He_{pw}$ and δ^2H profile shapes in the Lias-Dogger section, these profiles oftentimes increasingly diverge when approaching the hydrogeological boundaries.

Comparison of groundwater helium data in the Muschelkalk, Keuper and Malm aquifers with the porewater helium profiles shows three scenarios, with two being the result of diffusive redistribution of in-situ produced helium from the aquitards to the bounding groundwaters. A third scenario with groundwater helium concentrations clearly exceeding those of the aquitard porewater has been observed in the TRU1-1 borehole for the first time in any borehole in northern Switzerland. This scenario requires substantial addition of gas, including helium, to the groundwaters via some sort of pathway bypassing the aquitard sections in-between. Based on the $^3He/^4He$ signature of the observably helium enriched Keuper and Malm groundwaters, the sediments of the deep Permo-Carboniferous Trough underlying large portions of northern Switzerland have been identified as a possible external helium source, with deep-reaching tectonic structures such as the Neuhausen Fault potentially acting as such a cross-formational delivery pathway.

The present study provides a large dataset of helium concentration and $^3He/^4He$ ratios and demonstrates that the hydrogeological system across the central aquitard and the potential host rock for a nuclear waste repository is the result of a long-term evolution that resulted in a stable, diffusive transport controlled regime, presumably over very long time periods. Changes to the hydrological system bounding the aquitard have observable influences to the profile shapes of the porewater tracers close to these aquifers, without having yet an effect on the central part of the low-permeability rock sequence. A comprehensive, in-situ production, accumulation and diffusive transport study of the porewater evolution for selected boreholes using numerical modelling is planned.

Declaration of competing interest

The authors declare that they have no known competing financial interests or personal relationships that could have appeared to influence the work reported in this paper.

Data availability

Data will be made available on request.

Acknowledgements

All TBO drillcore sampling teams are gratefully acknowledged for delivering high quality noble gas samples and Nagra's TBO-G team, in particular M. Gysi, M. Stockhecke and H.P. Weber are thanked for their support and controlling function during the sampling campaigns. Groundwater ^4He and $^3He/^4He$ data were provided by E. Stopelli (Nagra) and G. Lorenz (Hydroisotop GmbH), which is highly appreciated. Analytical support for the determination of $^3He/^4He$ porewater ratios by J. Sültenfuss (University of Bremen, Germany) and the determination of ^4He porewater concentrations at the University of Bern by A. Kühnis, J. Hafner and D. Roos is appreciated. We thank the entire RWI Team at the University of Bern and M. Suchy for fruitful discussions and helpful comments over the course of this work as well as the two reviewers for their in-depth review and comments that helped improve the

manuscript. The project was carried out in the context of the Swiss deep drilling programme, financed by Nagra, Switzerland.

References

Andra, 2005. Dossier 2005 – Andra Research on the Geological Disposal of High-Level Long-Lived Radioactive Waste. Results and Perspectives. Technical Report Agence Nationale pour la Gestion de Déchets Radioactifs.

Ballentine, C.J., Burnard, P.G., 2002. Production, release and transport of noble gases in the continental crust. In: Porcelli, D., Ballentine, C.J., Wieler, R. (Eds.), Noble Gases in Geochemistry and Cosmochemistry, Reviews in Mineralogy & Geochemistry 47. Min. Soc. of America, Washington D.C., pp. 481–538

Battani, A., Smith, T., Robinet, J.C., Brulhet, J., Lavielle, B., Coelho, D., 2011. Contribution of logging tools to understanding helium porewater data across the Mesozoic sequence of the East of the Paris Basin. Geochim. Cosmochim. Acta 75, 7566–7584.

Bensenouci, F., Michelot, J.L., Matray, J.M., Savoye, S., Lavielle, B., Thomas, B., Dick, P., 2011. A profile of helium-4 concentration in pore-water for assessing the transport phenomena through an argillaceous formation (Tournemire, France). Phys. Chem. Earth 36, 1521–1530.

Bigler, T., Ihly, B., Lehmann, B.E., Waber, H.N., 2005. Helium Production and Transport in the Low-Permeability Callovo-Oxfordian Shale at the Site Meuse/Haute Marne, France. Nagra Arbeitsbericht NAB 05-07. Wettingen, Switzerland. www.nagra.ch.

Clark, I.D., Al, T., Jensen, M., Kennell, L., Mazurek, M., Mohapatra, R., Raven, K.G., 2013. Paleozoic-aged brine and authigenic helium preserved in an Ordovician shale aquiclude. Geology 41, 951–954.

Cook, P.G., Herczeg, A.L., 2000. Environmental Tracers in Subsurface Hydrology. Kluwer Academic Publishers, Boston, Dordrecht, London.

de Bievre, P., Peiser, H.S., 1992. Atomic weight: the name, its history, definition and units. Pure Appl. Chem. 64 (10), 1535–1543.

de Laeter, J.R., Böhlke, J.K., de Bièvre, P., Hidaka, H., Peiser, H.S., Rosman, K.J.R., Taylor, P.D.P., 2003. Atomic weights of the elements: Review 2000. Pure Appl. Chem. 75, 683–800.

Delay, J., Lesavre, A., Wileveau, Y., 2008. The French underground research laboratory in Bure as a precursor for deep geological repositories. In: Rempe, N. (Ed.), Deep Geologic Repositories, Reviews in Engineering Geology 19, pp. 97–111. https://doi.org/10.1130/2008.4119(10).

Gautschi, A., 2017. Safety-relevant hydrogeological properties of the claystone barrier of a Swiss radioactive waste repository: an evaluation using multiple lines of evidence. Grundwasser – Zeitschrift der Fachsektion Hydrogeologie. https://doi.org/10.1007/s00767-017-0364-1.

Gimmi, T., Aschwanden, L., Waber, H.N., Gaucher, E.C., Ma, J., Traber, D., 2023. Profiles of $\delta^{18}O$ and $\delta^{2}H$ in porewater of a Mesozoic rock sequence: Regional variability and relation to large-scale transport regimes. Appl. Geochem., 105846 https://doi.org/10.1016/j.apgeochem.2023.105846.

Gmünder, C., Malaguerra, F., Nusch, S., Traber, D., 2014. Regional Hydrogeological Model of Northern Switzerland. Nagra Arbeitsbericht NAB 13-23, Nagra, Wettingen, Switzerland. www.nagra.ch.

Hendry, M.J., Solomon, D.K., Person, M., Wassenaar, L.I., Gardner, W.P., Clark, I.D., Mayer, K.U., Kunimaru, T., Nakata, K., Hasegawa, T., 2015. Can argillaceous formations isolate nuclear waste? Insights from isotopic, noble gas, and geochemical profiles. Geofluids 15, 381–386. https://doi.org/10.1111/gfl.12132.

Jacops, E., Aertsens, M., Maes, N., Bruggeman, C., Swennen, R., Krooss, B., Amann-Hildenbrand, A., Littke, R., 2017. The dependency of diffusion coefficients and geometric factor on the size of the diffusing molecule: observations for different clay-based materials. Geofluids 2017. https://doi.org/10.1155/2017/8652560.

Jean-Baptiste, P., Lavielle, B., Fourré, E., Smith, T., Pagel, M., 2016. Vertical Distribution of Helium and $^{40}Ar/^{36}Ar$ in Porewaters of the Eastern Paris Basin (Bure/Haute Marne): Constraints on Transport Processes through the Sedimentary Sequence. Geological Society, London. Special Publications 443.

Kipfer, R., Aeschbach-Hertig, W., Peeters, F., Stute, M., 2002. Noble Gases in Lake and Ground Waters. In: Porcelli, D., Ballentine, C.J., Wieler, R. (Eds.), Noble Gases in Geochemistry and Cosmochemistry. Reviews in Mineralogy & Geochemistry 47. Min. Soc. of America, Washington D.C, pp. 615–700.

Madritsch, H., 2015. Outcrop-scale fracture systems in the Alpine foreland of central northern Switzerland: kinematics and tectonic context. Swiss J. Geosci. https://doi.org/10.1007/s00015-015-0203-2.

Mazurek, M., Alt-Epping, P., Bath, A., Gimmi, T., Waber, H.N., 2009. Natural Tracer Profiles across Argillaceous Formations: the CLAYTRAC Project. In: OECD/NEA Rep., vol. 6253. OECD Nuclear Energy Agency, Paris, France. www.oecdbookshop.org.

Mazurek, M., Alt-Epping, P., Bath, A., Gimmi, T., Waber, H.N., Buschaert, S., De Canniere, P., De Craen, M., Gautschi, A., Savoye, S., Vinsot, A., Wemaere, I., Wouters, L., 2011. Natural tracer profiles across argillaceous formations. Appl. Geochem. 26, 1035–1064.

Mazurek, M., Aschwanden, L., Camesi, L., Gimmi, T., Jenni, A., Kiczka, M., Mäder, U., Rufer, D., Waber, H.N., Wanner, P., Wersin, P., Traber, D., 2021. TBO Bülach-1-1 – data Report, Dossier VIII: rock properties, porewater characterisation and natural tracer profiles. Nagra Arbeitsbericht NAB 20-08. Nagra, Wettingen, Switzerland. www.nagra.ch.

Mazurek, M., Gimmi, T., Zwahlen, C., Aschwanden, L., Gaucher, E., Kiczka, M., Rufer, D., Wersin, P., Marques Fernandes, M., Glaus, M., Van Loon, L., Traber, D., Schnellmann, M., Vietor, T., 2023. Swiss deep drilling campaign 2019–2022: geological overview and rock properties with focus on porosity and pore geometry. Appl. Geochem., 105839 https://doi.org/10.1016/j.apgeochem.2023.105839.

McNaught, A.D., Wilkinson, A., 1997. Standard Pressure. IUPAC. Compendium of Chemical Terminology, (second ed.). Blackwell Scientific Publications, Oxford.

Meija, J., Coplen, T.B., Berglund, M., Brand, W., A, De Bièvre, P., Gröning, M., Holden, N. E., Irrgeher, J., Loss, R.D., Walczyk, T., Prohaska, T., 2016. Isotopic compositions of the elements 2013 (IUPAC technical report). Pure Appl. Chem. 88 (3), 293–306. https://doi.org/10.1515/pac-2015-0503.

Mohr, P.J., Newell, D.B., Taylor, B.N., 2016. CODATA recommended values of the fundamental physical constants: 2014. J. Phys. Chem. Ref. Data 45.

Nagra, 2002. Projekt Opalinuston: Synthese der geowissenschaftlichen Untersuchungsergebnisse. Nagra Technical Report NTB 02-03, Nagra, Wettingen, Switzerland. www.nagra.ch.

Nagra, 2001. Sondierbohrung Benken, Untersuchungsbericht. Nagra Technical Report NTB 00-01, Nagra, Wettingen, Switzerland. www.nagra.ch.

Nagra, 2014. SGT Etappe 2: Vorschlag weiter zu untersuchender geologischer Standortgebiete mit zugehörigen Standortarealen für die Oberflächenanlage. Geologische Grundlagen. Dossier VI: Hydrogeologische Verhältnisse. Nagra Technical Report NTB 14-02, Nagra, Wettingen, Switzerland. www.nagra.ch.

Ondraf/Niras, 2001. SAFIR 2, Safety Assessment and Feasibility Interim Report 2. Technical Report Ondraf/Niras, NIROND 2001-06 E, Brussels, Belgium.

Osenbrück, K., Lippmann, J., Sonntag, C., 1998. Dating very old pore waters in impermeable rocks by noble gas isotopes. Geochim. Cosmochim. Acta 62, 3041–3045.

Poole, J.C., McNeill, G.W., Langman, S.R., Dennis, F., 1997. Analysis of noble gases in water using a quadrupole mass spectrometer in static mode. Appl. Geochem. 12, 707–714.

Rübel, A.P., Sonntag, C., Lippmann, J., Pearson, F.J., Gautschi, A., 2002. Solute transport in formations of very low permeability: profiles of stable isotope and dissolved noble gas contents of pore water in the Opalinus Clay, Mont Terri, Switzerland. Geochim. Cosmochim. Acta 66, 1311–1321.

Rufer, D., Waber, H.N., 2015. Noble and Reactive Gas Data of Porewaters and Rocks from the Schlattingen Borehole SLA-1, Nagra Arbeitsbericht NAB 15-012. Nagra, Wettingen, Switzerland. www.nagra.ch.

Rufer, D., Waber, H.N., Gimmi, T., 2018. Identifying temporally and spatially changing boundary conditions at an aquifer – aquitard interface using helium in porewater. Appl. Geochem. 96, 62–77. https://doi.org/10.1016/j.apgeochem.2018.05.022.

Rufer, D., Stockhecke, M., 2021. Field Manual: Drill Core Sampling for Analytical Purposes. Nagra Arbeitsbericht NAB 19-13 Rev.1, Nagra. Wettingen, Switzerland. www.nagra.ch.

Sültenfuss, J., Roether, W., Rhein, M., 2009. The Bremen mass spectrometric facility for the measurement of helium isotopes, neon, and tritium in water. Isot. Environ. Health Stud. 45, 83–95.

Tolstikhin, I., Lehmann, B.E., Loosli, H.H., Gautschi, A., 1996. Helium and argon isotopes in rocks, minerals, and related groundwaters: a case study in northern Switzerland. Geochim. Cosmochim. Acta 60/9, 1497–1514.

Tolstikhin, I., Waber, H.N., Kamensky, I., Loosli, H.H., Skiba, V., Gannibal, M., 2011. Production, redistribution and loss of helium and argon isotopes in a thick sedimentary aquitard-aquifer system (Molasse Basin, Switzerland). Chem. Geol. 286, 48–58.

Tolstikhin, I., Tarakanov, S., Gannibal, M., 2018. Helium diffusivity and fluxes from a sedimentary basin (Permo-Carboniferous trough, Northern Switzerland). Chem. Geol. 486, 40–49.

Torgersen, T., 1980. Controls on pore-fluid concentration of ^{4}He and ^{222}Rn and the calculation of $^{4}He/^{222}Rn$ ages. J. Geochem. Explor. 13 (1), 57–75. https://doi.org/10.1016/0375-6742(80)90021-7.

Tyne, R.L., Barry, P.H., Cheng, A., Hillegonds, D.J., Kim, J.-H., McIntosh, J.C., Ballentine, C.J., 2022. Basin architecture controls on the chemical evolution and ^{4}He distribution of groundwater in the Paradox Basin. Earth Planet Sci. Lett. 589.

Van Loon, L., 2014. Effective diffusion coefficients and porosity values for argillaceous rocks and bentonite: measured and estimated values for the provisional safety analyses for SGT-E2. Nagra Technical Report NTB 12-03, Wettingen, Switzerland, p. 130. www.nagra.ch.

Van Loon, L.R., Bunic, P., Frick, S., Glaus, M.A., Wüst, R.A.J., 2023. Diffusion of HTO, ^{36}Cl and ^{22}Na in the Mesozoic rocks of Northern Switzerland. I: Effective diffusion coefficients and capacity factors across the heterogeneous sediment sequence. Appl. Geochem., 105843 https://doi.org/10.1016/j.apgeochem.2023.105843.

Waber, H.N., 2008. He in pore water. In: Waber, H.N. (Ed.), Borehole Oftringen: Mineralogy, Porosimetry, Geochemistry, Pore Water Chemistry. Nagra Arbeitsbericht NAB 08-18, Nagra, Wettingen, Switzerland. www.nagra.ch.

Waber, H.N., 2012. Laboratoire de Recherche Souterrain Meuse/Haute-Marne - Geochemical Data of Borehole EST433. Nagra Arbeitsbericht NAB 09-16, Nagra, Wettingen, Switzerland. www.nagra.ch.

Waber, H.N., Rufer, D., 2017. Porewater Geochemistry, Method Comparison and Opalinus Clay – Passwang Formation Interface Study at the Mont Terri URL. NWMO Technical Report TR-2017-10. Nuclear Waste Management Organization, Toronto, Canada. www.nwmo.ca.

Waber, H.N., Traber, D., 2022. Die Tiefengrundwässer in der Nordschweiz und im angrenzenden Süddeutschland: Beschaffenheit, Herkunft und unterirdische Verweilzeit. Nagra Technical Report NTB 19-02. Nagra, Wettingen, Switzerland. www.nagra.ch.

Waber, H.N., Traber, D., Stoppelli, E., 2023. TBO Trüllikon-1-1 (TRU1-1) Groundwater Hydrogeochemistry. Nagra Arbeitsbericht NAB 23-24, Nagra, Wettingen, Switzerland. www.nagra.ch.

Weiss, R.F., 1971. Solubility of helium and neon in water and seawater. J. Chem. Eng. Data 16, 235–241.

Wersin, P., Gimmi, T., Ma, J., Mazurek, M., Zwahlen, C., Aschwanden, L., Gaucher, E.C., Traber, D., 2023. Profiles of Cl and Br in boreholes penetrating the Mesozoic sequence in northern Switzerland. Appl. Geochem., 105845 https://doi.org/10.1016/j.apgeochem.2023.105845.